The challenging application of cosmogenic dating methods in residual glacial landforms: The case of Sierra Nevada (Spain)

David Palacios, Antonio Gómez-Ortiz, Jesús Alcalá-Reygosa, Nuria Andrés, Marc Oliva, Luis Tanarro, Ferran Salvador-Franch, Irene Schimmelpfennig, José M. Fernández-Fernández, Laëtitia Leanni

The challenging application of cosmogenic dating methods in residual glacial landforms: the case of Sierra Nevada (Spain)

David Palacios[a], Antonio Gómez-Ortiz[b], Jesús Alcalá-Reygosa[c], Nuria Andrés[a], Marc Oliva[b], Luis M. Tanarro[a], Ferran Salvador-Franch[b], Irene Schimmelpfennig[d], José M. Fernández-Fernández[a], Laëtitia Léanni[d], ASTER Team[de]

[a] Department of Geography, Universidad Complutense de Madrid, Madrid, Spain

[b] Department of Geography, Universitat de Barcelona, Barcelona, Spain

[c] Facultad de Filosofía y Letras, Universidad Nacional Autónoma de México, Ciudad de México, Mexico

[d] Aix-Marseille Université, CNRS, IRD, Coll. France, UM 34 CEREGE, Aix-en-Provence, France

[e] Consortium: Georges Aumaître, Didier Bourlès, Karim Keddadouche

Corresponding author: davidp@ucm.es (D. Palacios)

Abstract

An accurate review of the literature on surface exposure dating methods shows evidence of the difficulty in applying cosmogenic dating methods to old moraines because of the intensity of Late Quaternary erosion processes. Moreover, as in some previous cases, we found also special difficulties in applying these methods to LIA moraines, due to the intensity of current paraglacial processes. The objective of this study is to apply cosmogenic dating methods to very old and very young moraines, which in both cases have been or are being affected intensively by erosion. With this purpose, we collected samples of boulders from moraines corresponding to: (a) the penultimate glaciation, and (b) the Little Ice Age (LIA), both from Sierra Nevada, in the south of the Iberian Peninsula. The sampling strategy was based on a preliminary accurate analysis of the geomorphological settings of two valley sites that

resulted in the collection of only four boulder samples from an old moraine and three more from a very recent moraine. Using in situ produced cosmogenic ^{10}Be to date these boulders, the old samples yielded an age of ca. 130-135 ka for moraine stabilization. The younger samples indicate that the LIA moraine accretion probably occurred between the 14th and 17th centuries, with a subsequent stage of accumulation during the 19th century as suggested by historical documents. Both, dating a glaciation that occurred prior to the last Pleistocene glacial cycle and dating LIA glacial stages are novel in the context of Iberian glaciations and agree with other palaeoenvironmental studies in Iberian and in other European mountains. The limited number of boulders adequate for cosmic-ray exposure dating prevents statistical methods to be applied, and therefore highlights the need to improve geomorphological criteria in sample selection.

Key words: Sierra Nevada, cosmic-ray exposure dating, beryllium 10, Little Ice Age, Penultimate Glacial Cycle.

1. Introduction

Scientific knowledge on the glacial evolution of the Iberian mountains has greatly advanced over the last decade based on the application of Cosmic-Ray Exposure (CRE) dating on moraines, erratic boulders and polished surfaces. This method allowed inferring spatio-temporal patterns of glaciation since the maximum extent of glaciers during the last Pleistocene glacial cycle, with a focus on the Last Glacial Maximum (LGM) (García-Ruiz et al., 2010), Oldest Dryas (Palacios et al., 2017a) and Younger Dryas (García-Ruiz et al., 2016) in the main Iberian ranges such as the Cantabrian Mountains (Rodríguez-Rodríguez et al., 2016), Pyrenees (Delmas, 2015), Central System (Domínguez-Villar et al., 2013), Iberian System (Fernández-Fernández et al., 2017) and Sierra Nevada (Palacios et al., 2016).

The existence and distribution of landforms and deposits, their delimitation and mapping, generated by glacial advances prior to the last Pleistocene glaciation are known since the first geomorphological descriptions carried out in most Iberian mountains in the late 19th and early 20th centuries, such as in the Pyrenees (Penck, 1883; Nussbaum, 1949, Barrère, 1953), Cantabrian Mountains (Penck, 1897; Obermaier, 1914), Central System (Penck, 1897; Obermaier and Carandell, 1917) and Sierra Nevada (Quelle, 1908; Obermaier, 1916). However, the present knowledge on calendar of development of these landforms is scarce, and it is based on CRE dating only in very few cases. In fact, the only CRE data related to the penultimate glacial cycle were obtained with ^{21}Ne in the NW of the Iberian Peninsula (Vidal-Romaní, et al., 2015). These authors found glacial evidence (moraine boulders and polished surfaces) of a maximum advance that occurred at 155 ± 30 ka ^{21}Ne age in the Serra de Queixa, whereas polished bedrock surfaces were dated at 231 ± 48 ka and 131 ± 31 ka ^{21}Ne ages in the Serra da Geres. In addition, erratic blocks were dated at 113.9 ± 7.1 ka ^{10}Be age in the Porma Valley, Cantabrian Mountains (Rodríguez-Rodríguez et al, 2016). Another erratic boulder, with a minimum ^{10}Be age of 122.2 ± 4.9 ka was found in Ariège valley (northern Pyrenees) (Delmas et al., 2011). This scarcity of CRE data from old moraines may be due to the problem of moraine degradation after being affected by intensive erosion, as it has been observed even in younger moraines of other regions (Putkonen and Swanson, 2003; Briner et al., 2005; Putkonen et al., 2008; Balco, 2011; Heyman et al., 2011).

The rest of dates corresponding to glacial landforms formed during the penultimate glaciation in the Iberian Peninsula were carried out by other dating methods. Villa et al. (2013) were able to date with U / Th the limestone of cemented calcareous breccia in Duje valley, Picos de Europa, also in the Cantabrian Mountains. This breccia deposit lies on glacially abraded surfaces and is covered by moraines dated between 394 ± 50 ka and 276 ± 23 ka / 394 ± 50 ka U / Th age. In the southern slope of the Central Pyrenees, Optically Stimulated Luminescence

(OSL) dating was applied to sandy layers in fluvioglacial terraces in two nearby valleys that show the following ages: 151 ± 11 ka in the Gállego valley (Lewis et al., 2009) and 263 ± 21 ka and 171 ± 22 ka in the Aragón valley (García-Ruiz et al., 2013).

In other Mediterranean mountains, landforms originated from glaciations prior to the Late Pleistocene Glaciation (LPG) have been dated by U / Th, ^{230}Th and OSL methods in the Balkan region (Hughes et al., 2006a, 2006b, 2007), Dinaric Alps (Hughes et al., 2011) and Apennines (Kotarba et al., 2001), but not through CRE dating. In comparison to the large dataset of CRE ages existing for reconstructing the LPG in the Alps, there are only a few erratic boulders related to the penultimate glacial cycle dated by this method (Graf et al., 2015), as it is also the case of the Himalayas (Schaefer et al., 2008). On the contrary, the application of ^{230}Th-dates on the stalagmite record in the Alps allowed determining with high resolution the last maximum ice advance of the penultimate glacial cycle at 133.1 ± 0.7 and 131.9 ± 0.6 ka. These dates coincide with Heinrich stadial 11 and the onset of the penultimate deglaciation or Termination II (TII) which started at 131.8 ± 0.6 ka (Häuselmann et al., 2015) and reached its maximum intensity at 130.9 ± 0.9 ka (Moseley et al., 2015).

However, CRE methods have never been applied to date the Little Ice Age (LIA) in the Iberian Peninsula, although this cold event has been extensively documented in this region (González-Trueba et al., 2008; Oliva et al., 2018a). CRE dating showed that the LIA was the most extensive Holocene glacial advance in most Iberian mountains (Palacios et al., 2017b), with the exception of some cirques in the Central Pyrenees (García-Ruiz et al., 2014). In fact, after pioneer studies in New Zealand (Schaefer et al., 2009) and the Andes (Licciardi et al., 2009), the use of CRE dating methods to date landforms of Neoglacial and LIA age has just been recently applied in the Alps (Schimmelpfennig et al., 2012, 2014; Le Roy et al., 2017), Arctic (Jomelli et al., 2016; Young et al., 2015) and Central Asia mountains (Dong et al., 2017; Li et al., 2016).

Radiocarbon dating on glacial, fluvioglacial and lacustrine sediments, as well as speleothems, tree rings and historical documents established the onset of the LIA in the Iberian Peninsula at 1300 common era (CE), with the coldest conditions of ca. 2 ºC below present-day values at 1620-1715 CE and the last cold episodes at 1760-1800 and 1815-1835 CE (Oliva et al., 2018a). In Sierra Nevada there were also small glaciers during the LIA that have been reconstructed based on radiocarbon dating of lake sediments (Oliva and Gómez-Ortiz, 2012) and through historical documents (Gómez-Ortiz et al., 2009, 2018).

The objective of this work is to apply CRE methods to glacial landforms originated during advances prior to LPG and to very young moraines as well as to review and discuss those found in this research in comparison to other similar studies. Sierra Nevada constitutes a unique environment to examine the use of CRE dating as a potential tool to reconstruct the chronology of old and young glaciations, due to the well-constrained glacial chronological record of the LPG and the existence of glacial landforms originated before and after of this glaciation in this mountains.

2. Study area

Sierra Nevada is located in the SE of the Iberian Peninsula and runs SW-NE parallel to the Mediterranean Sea (Fig. 1). This massif includes the highest peaks of the Iberian Peninsula: Mulhacén (3478 m a.s.l.; 37°03'12"N, 3°18'41"W) and Veleta (3398 m; 37°03'02"N 3°20'54"W). The area is composed of Paleozoic metamorphic rocks, mainly micaschists, profoundly tectonized during the Alpine orogeny, with the presence of intensive foliation and joints that makes them susceptible to intense weathering (Messerli, 1965; Sanz de Galdeano and López-Garrido, 1999). Climate conditions in Sierra Nevada are characteristic of a semi-arid mid-latitude mountain environment, with a Mean Annual Air Temperature (MAAT) at 2500 m of 4.4 °C and a total precipitation of 710 mm, 40% of which as snow (Oliva et al.,

126 2016a). The MAAT at the top of the Veleta peak between 2002 and 2013 was 0.08 °C, with a
127 slight increase of 0.12 °C along this period (Oliva et al., 2016a).

128 The Quaternary landscape evolution of Sierra Nevada has been largely studied over the last
129 decades (Fig. 1, Table 1). From the first basic geomorphological observations of the late 19th
130 and early 20th centuries to the recent multi-dating approaches, our understanding of the glacial
131 processes shaping the landscape of the highest lands has significantly improved (i.e. Gómez-
132 Ortiz et al., 2015).

133 During the 1960s and 1970s several authors suggested the existence of older glaciations
134 occurred prior to the LPG, formerly known as the Riss glaciation in Alpine terminology.
135 Their observations focused on the existence of highly eroded moraine remnants and
136 fluvioglacial deposits at very low altitudes, mainly in the southern slope of the massif
137 (Hempel, 1960; Messerli, 1965; Lhenaff, 1977; Sánchez-Gómez, 1990). However, this
138 hypothesis has not been validated until now though direct dating methods.

139 By contrast, the LPG has been recently well-constrained with CRE techniques. Gómez-Ortiz
140 et al. (2012) and Palacios et al. (2016) reported two major glacial advances occurred at ca. 30-
141 32 ka and 19-20 ka. The second stage of glacial advance occurred in phase to the global Last
142 Glacial Maximum and reached almost the same extent than during the previous glacial stage.
143 Subsequently, temperature increase recorded worldwide (Clark et al., 2009) favored a massive
144 deglaciation of the massif, although two stages of glacial expansion occurred during the
145 transition towards the Holocene, namely during the Oldest Dryas and Younger Dryas. During
146 these phases, glaciers expanded significantly and flowed down-valleys several kilometers,
147 both in southern and northern slopes (Gómez-Ortiz et al., 2012; Palacios et al., 2016).

148 The Holocene was characterized by warmer temperatures that promoted the gradual melting
149 of these glaciers during the Early Holocene (Palacios et al., 2016). The formerly glaciated

150 environments were then subjected to paraglacial processes, which favoured the development
151 of rock glaciers associated to permafrost conditions (Oliva et al., 2016b; 2018b). These
152 permafrost-related landforms finally stabilized at 6-7 ka during the Holocene Climate
153 Optimum, when warmer conditions must have conditioned permafrost thawing (Palacios et
154 al., 2016).

155 Climate variability intensified in the Northern Hemisphere during the Late Holocene
156 (Mayewski et al., 2004). In Sierra Nevada, this was reflected in alternating cold and warm
157 phases (Oliva et al., 2014). During the coldest stages, some glacier spots developed in the
158 highest northern cirques, such as in the Mulhacén cirque, where lake sediments from La
159 Mosca Lake revealed evidence of the existence of a glacier within the cirque at ca. 2.8-2.7 ka
160 cal BP, 1.4-1.2 ka cal BP, and during the LIA between 1440 and 1710 CE (Oliva and Gómez-
161 Ortiz, 2012). For the last cold stage, historical documents also showed evidence of the
162 prevailing colder conditions in Sierra Nevada, with descriptions, sketches and pictures of
163 glaciers and permanent snow fields at the foot of the highest peaks of the westernmost
164 mountains of Sierra Nevada between the late 17th and the early 20th century. The last glacier
165 was located in the Veleta cirque and constituted the southernmost glacier in Europe during the
166 LIA, although it finally melted away during the mid-20th century (Gómez-Ortiz et al., 2001,
167 2009, 2018; Oliva and Gómez-Ortiz, 2012; Oliva et al., 2018a). However, no CRE dating is
168 yet available from the different LIA glacial stages in Sierra Nevada.

169 **3. Methods**

170 *3.1 Sampling strategy*

171 With the aim of dating glacial landforms formed potentially before the LPG, this research
172 focuses on the Naute valley, a steep mountain ravine located on the southern slope of the
173 Mulhacén peak (Fig. 1, 2, 3 and 4). The valley results from the confluence of two glacial

174 headwaters –Río Seco and Mulhacén valleys– converging at 2300 m of altitude. In previous
175 studies these two high mountain valleys were selected to reconstruct glacial stages of the LPG
176 using CRE methods (Gómez-Ortiz et al., 2012; Palacios et al., 2016), but landforms
177 distributed in the lower Naute valley affected by intense erosion processes were not
178 examined. In Río Seco and Mulhacén valleys landforms from the LPG have been already
179 dated using the *in situ* cosmogenic nuclide ^{36}Cl , such as the front of a fossil rock glacier (9.0
180 ± 0.8 ka) resting on polished rock surfaces (11.9 ± 1.1 ka) in the Río Seco cirque, as well as of
181 a fossil rock glacier (6.3 ± 0.5 ka and 13.1 ± 1.3 ka) resting on a polished rock surface (11.2 ±
182 1.1 ka and 12.7 ± 1.2 ka) at the head of the Mulhacén valley (Palacios et al., 2016). Just
183 before their confluence, both valleys include a sequence of moraine ridges, where 5 blocks
184 were dated using ^{36}Cl (29.9 ± 2.6 ka, 16.9 ± 1.8 ka, 14.9 ± 1.5 ka, 13.7 ± 1.3 ka, 11.7 ± 1.6 ka;
185 Palacios et al., 2016). These authors interpreted these ridges as a polygenic moraine formed
186 by successive advances generated from just before the LGM to the Oldest Dryas. In the Naute
187 valley, immediately below the confluence of these two tributaries, a lateral moraine is
188 preserved in the left sector of the valley at elevations between 2150 and 2300 m. This moraine
189 is placed below one of the ridges where a boulder was dated at 29.9 ± 2.6 ka (Palacios et al.,
190 2016), and therefore must be older in age, possibly from a previous glaciation. For this
191 reason, this lower moraine was considered as one of the objectives of the work, in order to
192 apply the CRE dating method.

193 To date glacial oscillations during the LIA by CRE dating methods, we focused our research
194 on the Veleta cirque, located under the northern wall of Veleta peak (Fig. 1, 5, 6). Historical
195 documents provided abundant evidence of a glacier existing at the floor of this cirque during
196 the LIA until the first half of the 20th century (Gómez-Ortiz et al., 2001, 2009, 2018). The
197 cirque is closed by a large frontal moraine whose age is unknown, although due to its large

size it has been considered to have formed during the Last Termination or during Holocene advances (Oliva et al., 2014, 2018a).

3.2 Sampling and analytical procedures

Seven samples were collected from moraine boulders using a hammer and a chisel: four located in Naute valley (NAUT-1, -2, -3, -4) between 2164 and 2263 m, and three in the Veleta cirque (SN-11-1, -2, -3) between 3061 and 3095 m (Table 1). All samples were taken from the flat-topped surfaces of boulders > 1 m high, located on the crests of the moraines. Field data and sample characteristics of the seven samples are listed in Table 2.

Physical and chemical sample preparation and beryllium measurements were carried out at the Centre Européen de Recherche et d'Enseignement des Géosciences de l'Environnement (CEREGE, France). Lichen, moss and other organic fragments were removed from the samples with a brush. Samples were crushed with a roller grinder and sieved to retrieve the grain size fraction 0.25–1 mm. All samples are quartz-bearing micaschists, and therefore we selected in situ-produced cosmogenic ^{10}Be dating to determine the ages of the moraines. To isolate the quartz from the bulk rock, the samples went repeatedly through a magnetic separator (Frantz LB-1) until all magnetic minerals were discarded. Subsequently, the non-magnetic fraction experienced successive chemical attacks with a mixture of concentrated hydrochloric (HCl) and hexafluorosilic (H_2SiF_6) acids to dissolve the remaining non-quartz minerals. The residual impurities were dissolved when the sample grains were decontaminated from meteoric ^{10}Be by three successive partial dissolutions with concentrated hydrofluoric acid (HF).

The subsequent beryllium extraction protocol is adapted from Brown et al. (1991) and Merchel and Herpers (1999) chemical procedures. The samples yielded between 18 and 32 g of purified quartz (Table 3). About 100 µl of a ^{9}Be carrier solution with a ^{9}Be concentration of

222 3025 µg/g prepared in-house from a phenakite crystal was added to the quartz before it was
223 dissolved in HF. A chemistry blank was prepared along with the seven samples. Following
224 evaporation of the resulting solution, the samples were recovered in a hydrochloric acid
225 solution and beryllium was precipitated to $Be(OH)_2$ with ammonia before and after elution
226 through an anionic exchange column (Dowex 1X8) to remove iron. Following the methods
227 described by Merchel and Herpers (1999), a cationic exchange column (Dowex 50WX8) was
228 used to remove boron and to separate the Be from other elements. Beryllium was precipitated
229 with ammonia to $Be(OH)_2$ and the resulting precipitate was oxidized to BeO at 700 °C. Then,
230 this final BeO was mixed with niobium powder and loaded on cathodes for analysis of the
231 $^{10}Be/^{9}Be$ ratios at the French national Accelerator Mass Spectrometry (AMS) facility ASTER
232 (CEREGE) (Arnold et al., 2010). The measurements were calibrated against in-house
233 standard STD-11 using an assigned $^{10}Be/^{9}Be$ ratio of 1.191 (±0.013) x 10^{-11} (Braucher et al.,
234 2015). Sample $^{10}Be/^{9}Be$ ratios were corrected for the chemical blank background by
235 subtracting the measured chemistry blank $^{10}Be/^{9}Be$ ratio (Table 3). Analytical 1 sigma
236 uncertainties include uncertainties in AMS counting statistics, the uncertainty in the standard
237 $^{10}Be/^{9}Be$ ratio, an external AMS error of 0.5% (Arnold et al., 2010), and the uncertainty in the
238 chemical blank measurement. A ^{10}Be half-life of 1.387 (± 0.01) x 10^{6} years was used
239 (Chmeleff et al., 2010; Korschinek et al., 2010).

240 *3.3 Age calculation (^{10}Be age computation)*

241 We calculated the ^{10}Be CRE ages with the online CREP exposure age calculator (Martin et
242 al., 2017; http://crep.crpg.cnrs-nancy.fr), using the LSD scaling model (Lifton et al., 2014)
243 that is similar to other previous empirical models (Borchers et al., 2016). Age calculations
244 have also considered the ERA40 atmospheric model (Uppala et al., 2005) and LSD
245 Framework geomagnetic database (Lifton et al., 2014). As there is no regional production rate
246 available, we used the worldwide mean ^{10}Be spallation production rate of 3.99 ± 0.22 atoms g^{-}

247 ^{1} yr^{-1}, as calibrated in the ICE-D production rate database linked to CREp. For all samples, a
248 rock density of 2.7 g cm^{-3} was considered and the topographic shielding factor of each sample
249 was calculated (Table 2).

250 In the moraine of the Veleta cirque, from where samples SN-11-1, SN-11-2 and SN-11-3
251 were extracted, snow cover remains for a large part of the year (Gómez-Ortiz et al., 2009),
252 and there is information on the properties and persistence of the snow cover for the last
253 decades (Herrero and Polo, 2016), which allows considering snow shielding effect for these
254 samples. The correction for snow cover has been calculated applying the equation by Gosse
255 and Phillips (2001), including local parameters (Herrero and Polo, 2016), and considering a
256 snow thickness on moraine boulders ranging from 30 to 130 cm during 8 months per year. We
257 used an average value of snow density of 0.3 g cm^{-3}, considering that the attenuation length
258 for fast neutrons in snow is 109 g cm^{-2} (Zweck et al., 2013; Delunel et al., 2014). Taking into
259 account these characteristics, we applied a snow shielding factor of 0.865 to the affected
260 samples. We have not applied a snow shielding factor to the old samples of Naute moraine,
261 since the coverage of snow in this area is much shorter and data are not available for a period
262 encompassing several tens of thousands of years.

263 Table 3 also includes the ages determined with version 3 of the online exposure age calculator
264 formerly known as the CRONUS-Earth online exposure age calculator (Balco et al., 2008;
265 Balco, 2018). These ages have been calculated using the default calibration data set based on
266 the ICE-D calibration database and the time-dependent "LSDn" scaling method (Lifton et al.,
267 2014). The average difference between the ages calculated with the CREP exposure age
268 calculator and those calculated with the CRONUS-Earth (v.3) is 2.4% for NAUT samples and
269 6.9% for SN-11 samples.

270 The ages of the SN-11 samples calculated with the snow shielding factor turn out to be
271 between 8.8 and 16.9% higher in the online CREP exposure age calculator (Martin et al.,

272 2017) and between the 7.9 and 16.9% higher in the online exposure age calculator formerly
273 known as the CRONUS-Earth online exposure age calculator v. 3 (Balco et al., 2008; Balco,
274 2018). The CREP exposure calculator ages and the analytical uncertainties are used in the text
275 and in the figures of this manuscript and, only in the case of the Veleta cirque, with the
276 application of the snow shielding factor (Table 3).

277

278 **4. Results**

279 *4.1 Geomorphological analysis of the Naute moraine and CRE dating results*

280 To select the most suitable boulders for CRE dating, an exhaustive survey was carried out of
281 the Naute moraine system, formed potentially during a glacial advance before the LPG. The
282 results of this survey are expressed in a detailed geomorphological map (Fig. 2). The moraine
283 is located on the left bank of the Naute river (west) and the Peñón Grande (east) between
284 2150 and 2300 m. It has been intensely reshaped by postglacial environmental dynamics: (i)
285 fluvial processes driven by steep streams have deeply eroded the moraine ridge, and (ii)
286 gullying processes have washed away a large part of its abundant fine sediments. As a result,
287 a large number of boulders -highly weathered and fragmented due to their abundant foliation
288 planes and joints- are found on the surface of the moraine (Fig. 3).
289 To sample the boulders that best represent the original surface of the moraine, we focused on
290 blocks that: (i) present aligned upper edges indicating the maximum possible height of the
291 original moraine crest, and (ii) are inserted into the moraine, which ensures that they have not
292 been mobilized since the moraine stabilization. Using these criteria, only four boulders were
293 found with these characteristics (NAUT-1, 2, 3 and 4) (Fig. 4). The rest of the boulders
294 showed traces of having been affected by erosion and exhumed.

Samples from two boulders showed a similar age: NAUT-1 yielded 134.8 ± 6.2 ka and NAUT-4 129.2 ± 5.3 ka. The other two boulders showed different and substantially younger ages: NAUT-2 obtained 53.7 ± 2.9 ka and NAUT-4 43.8 ± 2.3 ka (Figs 2, 3 and Table 3).

4.2 Geomorphological analysis of the Veleta cirque moraine and CRE dating results

The Veleta cirque moraine is composed of a large proportion of fine sediments with a few large blocks on the surface, possibly deposited by different glacial advances. Within the area enclosed by this moraine, there are large rock avalanche deposits fallen from the Veleta northern wall and a small rock-glacier where buried glacial ice is still preserved under the debris cover, though it presents evidence of accelerated degradation. On the other hand, the fine sediments of the moraine, resulting from heavily weathered micaschists, are being washed away by runoff activity. This process is particularly intense in late spring and early summer with snowmelt runoff, and in autumn with torrential rain events. The outer slope of the moraine is being reshaped by frequent debris flows, which also facilitate the outcropping and exhumation of large blocks buried in the moraine. In addition, there are some metric-size boulders fallen from the Veleta north wall and deposited on the surface of the moraine, normally during the winter season when snow completely fills the floor of the cirque. These rocks slide on the snow and ice surface and stabilize on the moraine ridge. On the inner slope of the moraine, accumulations are found of superimposed till blocks of different sizes. In contrast to the main moraine, these till deposits include a smaller proportion of fine particles but conserve a recent glacial imprint as revealed by the presence of flutes. This deposit exceeds the limits of the main moraine on the eastern side of the cirque, where the moraine height is lower (Fig. 5 and 6). Evidence from historical sources confirms that the distribution of this recent till deposit coincides with the surface covered by the glacier during the 19th century (Fig. 7; Bide, 1893; Gómez-Ortiz et al., 2018).

Before selecting boulders for CRE dating, a very detailed geomorphological survey of the large polygenic moraine system enclosing the Veleta cirque was conducted. A detailed geomorphological map shows the main landforms observed in the cirque (Fig. 5). Schematic transects show the sectors of the moraine affected by current or recent post-glacial processes and derived landforms (Fig. 6). Considering these geomorphological characteristics, we avoided collecting samples from blocks corresponding to very recently deglaciated surfaces because: (i) we already know that this area was occupied by the glacier during the 19th century and (ii) they can result from the frequent rockfalls from the headwall. As a result, only three CRE datable boulders were found anchored in the moraine and protruding sufficiently not to have been covered by other sediments since their deposition (SN11-1, 2 and 3) (Fig. 7). Thus, they cannot have fallen from the headwall, or have been covered by the glacier in a subsequent readvance.

Sample SN-11-1, collected on the top of the moraine, very close to 20th century till deposits, obtained an age of 340 ± 120 years, corresponding to the year 1675 ± 120 CE. Sample SN-11-2, collected on the crest of the lobate ridge of the moraine, yielded an age of 720 ± 270 years (1295 ± 270 CE). Finally, sample SN-11-3, collected on the top of the lateral moraine ridge in the western part of the cirque, obtained an age of 400 ± 110 years (1615 ± 110 CE) (Figs 5, 6 and Table 3).

5. Discussion

5.1 The existence of a glaciation prior to the last Pleistocene glaciation in Sierra Nevada

The results of ^{10}Be CRE dating yielded ages of ca. 130-135 ka for the two samples collected from boulders in the moraine downslope of the maximum ice advance in Sierra Nevada (Gómez-Ortiz et al., 2012). These ages suggest that the moraine may have been formed during the last maximum advance of the penultimate glaciation. The other two boulders of the

same moraine yield much younger ages, around 45-50 ka (Table 3), and thus can be considered outliers. On the other hand, none of the studies in Sierra Nevada reported boulder samples affected by nuclide inheritance (Gómez-Ortiz et al., 2012; 2015; Palacios et al., 2016), and therefore this problem can be rejected in the older samples.

In Sierra Nevada, no surfaces polished and striated bedrock surfaces where found in this study between the moraine ridges dated ca. 130-135 ka and those dated in previous studies between ca. 30 and ca. 15 ka (Palacios et al., 2016), i.e. rock surfaces which may have been ice-covered prior to the LPG. All the polished bedrock surfaces dated in Sierra Nevada –in many cases with abundant and well-preserved fresh striations– correspond to the deglaciation process during Termination I (Gómez-Ortiz et al., 2012; Palacios et al., 2016). The fact that moraines from a previous glaciation are found in close proximity to those of the last glacial cycle without intermediate polished surfaces led us to apply CRE dating only on boulder surfaces in the old moraines. Recent research in mountain areas, such as in the Alps (e.g. Chenet et al., 2016), the Andes (e.g. Martini et al., 2017), Central Asia (e.g. Batbaatar et al., 2018) and the Iberian Peninsula (Rodríguez-Rodríguez et al., 2016, 2017), suggest using a minimum of 5 boulders from the same moraine to ensure obtaining the formation age of the landform. Thus, where most of the results show dispersed data, the ages are rejected, whereas an average value is obtained with the rest, interpreted as indicative of the development age of the moraine. In this study we attempted to apply this five-boulder criterion, but this proved impossible due to the deterioration of the moraine since the penultimate glaciation, as the landform has been intensely eroded and few potentially datable boulders are available. The headwaters of several torrents have eroded the ridge summit, leaving the moraine covered with loose blocks. When trying to reconstruct the original surface of the moraine we found only four embedded boulders (Fig. 4).

The CRE ages of ca. 130-135 ka obtained in Sierra Nevada coincide with the last cold period of the penultimate glaciation in the Alps as suggested by ^{230}Th dating on speleothems that obtained 131.8 ± 0.6 ka (Häuselmann et al., 2015; Moseley et al., 2015). This stage occurred during Heinrich stadial 11 (Oppo et al., 2006), parallel to the end of the last cold phase in the Alboran sea surface temperatures (near Sierra Nevada, in SE Iberia) before the beginning of TII (Martrat et al., 2014; Jiménez-Amat and Zahn, 2015). By that time, the onset of warmer temperatures favored the end of the last cold period of the penultimate glaciation in Greenland (Grant et al., 2012) as well as the initial melting of large ice sheets at high latitudes in the Northern Hemisphere (Govin et al., 2015), leading to sea level rise (Rohling et al., 2017).

The formation and stabilization of the Naute moraine may therefore be contemporary with what is called the Penultimate Glacial Maximum (PGM), a parallel concept to the LGM for the last glaciation, centered on 140 ka (Rohling et al., 2017). The deposition age of the Naute moraine is similar to the stabilization age of the maximum glacial advance moraine in the Sierra de Queixa dated 155 ± 30 ka ^{21}Ne (Vidal-Romaní et al., 2015). The erratic boulder dated 113.9 ± 7.1 ka ^{10}Be in the Porma Valley, Cantabrian Mountains, could also be related to the deglaciation process following the PGM (Rodríguez-Rodríguez et al., 2016). The same is true for the erratic boulder in the Ariège valley (northern Pyrenees), with a minimum ^{10}Be age of 122.2 ± 4.9 ka (Delmas et al., 2011), slightly after the formation of the Naute moraine from the penultimate glaciation. In addition, fluvioglacial terraces deposited simultaneously on the outermost moraine ridges in the Gállego and Aragón valleys, Central Pyrenees, were dated 151 ± 11ka and 171 ± 22 ka OSL ages by other authors (Lewis et al., 2009; García-Ruiz et al., 2013), and therefore may represent the same glacial stage that led to the formation of the Naute moraine. However, despite some evidence suggesting glacial activity between ca. 170 and 130 ka in the Iberian Peninsula, the small number of reliably dated terrestial records makes it difficult to infer spatiotemporal glaciation patterns occurring before the LPG. This is

392 a common issue in other Mediterranean mountains where glacial advances concurrent with
393 the development of the Naute moraine have only been dated through the application of U
394 series to secondary carbonates in cemented moraines in mountains in Greece (Hughes et al.,
395 2006a, b, 2007), Dinaric Alps (Hughes et al., 2007) and the Gran Sasso Massif, Central Italy
396 (Kotarba et al., 2001).

397 A case study similar to the Naute moraine was undertaken in the Jura mountains, where
398 several erratic boulders were found scattered beyond the Alpine glaciers LGM extent. In this
399 case the oldest ages were very similar to those of the Naute moraine (129.7 ± 4.7 ka, 143.2 ±
400 8.2 ka and 144.0 ± 5.3 ka ^{10}Be ages), although just as in Sierra Nevada, other boulders in the
401 same deposit yielded younger ages (Graf et al., 2015). After their experience applying CRE
402 dating to several moraine boulders in the Himalayas, Schaefer et al. (2008) highlighted the
403 role of erosion processes in the exhumation of blocks in old moraines. As a result, these
404 authors claim that the oldest, not the average age of the moraine boulders reflects the best
405 minimum age estimation for the moraine deposition, in agreement with previous authors
406 (Hallet and Putkonen, 1994). Briner et al. (2005) proposed the same criterion after analyzing a
407 large number of moraine boulders, presumably from the penultimate glaciation in Alaska, and
408 found many problems of boulder exhumations. These authors also defend an "oldest-age
409 method" to provide the closest approximation to the moraine stabilization age. Similarly, and
410 from previous experience, Balco (2011) defined the most appropriate strategies when
411 applying CRE methods to degraded moraines, which have been considered in this study.

412 From our results we conclude that the difficulty of finding suitable boulders to apply CRE
413 methods in moraines from old glaciations should not discourage their use. Dating an adequate
414 number of samples is very difficult for moraines prior to the LPG, where erosive activity over
415 time may have exhumed most of the boulders. In the case of Sierra Nevada, the profoundly
416 tectonized micaschists have been intensely affected by erosion, which makes it more difficult

417 to find suitable boulders for dating (Gómez-Ortiz et al., 2015). Nevertheless, Sierra Nevada is
418 an arid mountain, where ice margin deposits preserved on gentle slopes make it possible to
419 obtain a well-dated glacial sequence using the CRE method (Pallàs et al., 2010) (Fig. 9).

420 *5.2 Chronology of LIA moraine formation in Sierra Nevada*

421 It was also difficult to find suitable blocks for CRE dating in young moraines in Sierra
422 Nevada, as they are found in very dynamic geomorphological environments on steep slopes of
423 200 m high (up to 300 m from the peaks to the cirque floors) with thick and long-lasting snow
424 cover. On the one hand, these factors accelerate erosion processes in the moraine, often
425 reducing its size, vertical development and the slope gradient; on the other hand, they favor
426 new sediment deposits on the moraine surface. These difficulties are also observed in most
427 Mediterranean mountains, where LIA glaciers did not exceed the limits of the cirques and
428 developed at the foot of vertical walls (Hughes, 2014, 2018). Previous studies adverted to the
429 polygenic character of the Veleta cirque moraine, related to the effects of an Early Holocene
430 glacial advance that pushed downslope, accumulating rockfall deposits from the end of TI
431 (Gómez-Ortiz et al., 2012; Palacios et al., 2016). According to these authors, this moraine
432 system functioned as a barrier to subsequent advances, which accumulated sediments on the
433 inner slope, generating a single, large, polygenic moraine.

434 Using the criteria defined in Methods above, we obtained three coherent results to infer the
435 age of the moraine, although dates were obtained for only three boulders. The high
436 uncertainty levels in our results prevent us from relating the age of each sample to LIA
437 periods (Oliva et al., 2018a). These ages could be related to advances from 1300 CE to
438 1610/1680 CE, contemporary with the LIA maximum glacial advance in the Alps
439 (Holzhauser et al., 2005) and the lowest temperatures in the Iberian Peninsula during the
440 Maunder Minimum (Oliva et al., 2018a).

441 The inner slope of the moraine therefore developed during the LIA, although the large
442 moraine system may also include boulders from other Neoglacial glacial stages, such as those
443 detected in the Mulhacén cirque, where lake sediments show evidence of a glacier within the
444 cirque ca. 2.8-2.7 ka, 1.4-1.2 ka cal BP and LIA (Oliva and Gómez-Ortiz, 2012).

445 New results obtained in Mount Olympus (Greece) found similar results using ^{36}Cl dating
446 method, with one sample of 0.64 ± 0.08 ka (Styllas et al., 2018). However, most studies
447 focusing on the use of CRE dating methods for dating LIA glacial advances have been carried
448 out in the Alps. In the Western Alps, LIA moraines are very close to Neoglacial (Late
449 Holocene) moraines and may even overlap them (Schimmelpfennig et al., 2012; 2014); as in
450 the Veleta cirque, LIA glacial advances have left a single polygenic ridge with dated boulders
451 showing a wide range of dates: 1430 ± 32, 1534 ± 28, and 1829 ± 11 CE ^{10}Be (ages not
452 considering snow shielding) (Schimmelpfennig et al., 2012). These dates could correspond to
453 the three most important glacial advances in the Alps during the LIA: 1300-1380, 1600-1670
454 and 1800-1860 CE (Holzhauser et al., 2005), similar to those detected in the Pyrenees (Oliva
455 et al., 2018a). Recent studies in the Central Alps showed a similar pattern when dating LIA
456 moraine boulders –also very close to or overlapping Neoglacial moraines–forming single
457 polygenic crests (Schimmelpfennig et al., 2014). These authors dated 14 boulders in a single
458 LIA moraine ridge using ^{10}Be, assuming negligible inheritance for the boulders, and reported
459 dates ranging from 1430 to 1870 CE (Schimmelpfennig et al., 2014). Le Roy et al. (2017)
460 dated Neoglacial moraines near several present-day glacier fronts in the French Alps and
461 obtained ^{10}Be ages that are all consistent with the Late Holocene period (~4-1 ka), but do not
462 follow the logical chronostratigraphic moraine sequence. These authors highlighted the
463 problems related to surface exhumation and erosion of many moraine ridges.

464 Some attempts to date the moraines of the LIA have been also made in other high mountain
465 ranges such as the Cordillera Vilcabamba, Central Andes where Licciardi et al. (2009) applied

466 ^{10}Be CRE dating for the first time. Samples collected from a single massive ridge showed
467 average dates ranging from 1740 ± 30 to 1810 ± 20 CE, though samples of old dates were
468 rejected as being outliers. They suggest that the moraines found in several valleys of this
469 massif may be the result of the successive accumulation of multiple Late Holocene glacial
470 expansions.

471 Schaefer et al. (2009) also applied ^{10}Be dating in the Mueller valley in the Southern Alps,
472 New Zealand, to date many LIA moraine boulders. The geomorphological setting is similar to
473 that described in the European Alps, with a single LIA moraine system overlapping with
474 various Late Holocene moraine ridges. Boulders taken from different sites in the LIA moraine
475 reported dates of 1350 ± 60, 1600 ± 50, 1780 ± 40 and 1820 ± 20 CE ^{10}Be, which coincide
476 with cold periods inferred from tree-ring data. Li et al. (2016) applied ^{10}Be dating in LIA
477 moraines in Tian Shan mountains, Central Asia; interestingly, they found that boulders in
478 moraines from glaciers smaller than 1.0 km^2 show very old ages because of nuclide
479 inheritance. The same problems were found in the small Veleta cirque, where the wall is very
480 close to the moraine, but we discarded this possibility following the results obtained in this
481 present study and those from other previous work in Sierra Nevada, because of the intense,
482 continuous rock fall activity on its wall. For larger glaciers, Li et al. (2016) found evidence of
483 a major advance ca. 1600 ± 100 CE ^{10}Be, and also a remarkable early LIA glacial expansion
484 at ca. 1480 ± 55 CE ^{10}Be. Dong et al. (2017) dated two different LIA ridges in Tibetan
485 mountains with ^{10}Be, collecting four samples from each ridge. Their results provide a range of
486 1480±139 to 1975±31 CE ^{10}Be dates for the entire moraine system, very similar to the Veleta
487 cirque results. Young et al. (2015) dated several stable moraine ridges close to the current
488 alpine glacier snouts in Baffin Island and western Greenland and found a logical
489 geomorphological order from 1040±40 CE to 1700±40 CE ^{10}Be ages with a retreat from 1750
490 CE, and proposed a recent glacial maximum during the Medieval Climate Anomaly, when

glaciers in Europe receded. Jomelli et al. (2016) applied in situ cosmogenic ^{36}Cl to date three moraines in Lyngmarksbræen glacier (West Greenland), which were deposited during the last millennium in a relatively flat area not constrained by topography, the opposite that happens in Alpine environments. These authors obtained advances with average ages of 1200 ± 130 CE, 1450 ± 90 CE and 1720 ± 60 CE for the most external and internal ridges. The most recent advances coincide with glacial expansion in European high mountains, but the older moraine may have developed during the Medieval Climate Anomaly (Jomelli et al., 2016). In the sub-Antarctic Kerguelen islands, Jomelli et al. (2017) recently dated a moraine with ^{36}Cl that is probably related to the LIA.

From a review of the available literature on LIA moraine dating in different mountain ranges, we concluded that, in general, a first glacial advance was recorded during the 14th century, with the major ice expansion during the 17th century and a last minor readvance at the beginning of the 19th century.

Due to the short exposure duration of our samples, their ^{10}Be ages have 25-30% analytical uncertainties. These uncertainties are higher than the age difference of 10-16% obtained when a snow shielding correction factor is applied, as was proposed in early studies (Benson et al., 2004; Schildgen et al., 2005). In any case, this study defends the importance of considering the snow cover of the moraines studied, both when applying CRE methods, and to discover the degree of degradation to which they have been subjected. The location of the glacial fronts during the LIA suggests MAAT ca. 1 ºC below current values in mid-latitude mountain regions (Oliva et al., 2018a), determining longer snow cover duration in the highlands of the glaciated massifs and strengthening shielding from cosmogenic radiation (Fig. 7). Long-lasting snow cover also intensifies nivation-related erosion processes and can intensely affect glacial deposits (Christiansen, 1998; Palacios et al., 2003).

On the other hand, as we observed in the Veleta cirque, and as described in several papers cited above, the intensity of the paraglacial processes (Ballantyne, 2002; Oliva and Ruiz-Fernández, 2015) in the current deglaciation phase from the LIA advance is very high, with a complex superposition of processes that destroy the glacial landforms and accumulate new deposits on them. Therefore, as we saw, it was difficult to find suitable boulders for CRE dating in the Veleta cirque, despite its young age. In this context, the long-term study and monitoring of the dynamics of the LIA moraines in full paraglacial phase, should serve to evaluate the time needed for moraine stabilization, once it has been abandoned by glacial retreat (Zreda and Phillips, 1994,1995; Putkonen and O'Neal, 2006; Putkonen et al., 2008; Heyman et al., 2011) (Fig. 9).

In areas where LIA moraines are constrained by steep slopes, as is very common in Alpine systems, at least two, or possibly three, major LIA advances overlap, in some cases with other Neoglacial moraines, to form a single polygenic ridge, as occurred in the Veleta cirque. This was highlighted in the mid-1980s with the concepts of "obliterative overlap" (Gibbons et al., 1984) and "distal-flank accretion" (Osborn, 1986) applied to Neoglacial advances.

6. Conclusions

The results of this research supply evidence of the very few CRE dates available on very old glacial landforms formed before the last Pleistocene glaciation, and also the few very young dates available, such as those derived from LIA glaciation, compared with the large number of dates obtained for Termination I. For both periods, the selection of boulders suitable for sampling was the critical issue in Sierra Nevada, due to intense postglacial environmental dynamics such as occurred during the last major deglaciation, which impedes the collection of a statistically significant number of samples. In the case of the LIA, moraines are still undergoing intense paraglacial readjustment to the new geomorphological setting, with very intense erosion and sediment redistribution of the unconsolidated moraine particles. In

addition, moraine accretion processes during successive glacial advances are detected from geomorphological observations. In moraines originating during the penultimate glaciation, the long time lapse since their formation has facilitated intense erosion and reshaping of these landforms, with very few stable blocks remaining on the surface since their original stabilization. Periods of certain geomorphic stability may have occurred between the very old and the younger glaciations (Fig. 9).

The results of this research have enabled us to verify the existence of moraines deposited in glaciations prior to LPG in Sierra Nevada, as many of the first geomorphologists who studied the glacial landforms of this mountains suggested, and confirm similar CRE and OSL ages established in other mountains in the northern Iberian Peninsula.

In addition, CRE dates are obtained for the first time in the Iberian Peninsula in LIA moraines, with results suggesting that maximum advances during this period occurred between the 14^{th} and 17^{th} centuries, as is the case in many other mountains where the same method has been applied.

Acknowledgments

The research was carried out within the MOUNTAIN WARMING project (CGL2015-65813-R). Marc Oliva is grateful for the support of the Ramón y Cajal research program (RYC-2015-17597) and the ANTALP research group (Antarctic, Arctic, Alpine Environments, 2017-SGR-1102). The ^{10}Be measurements were performed at the ASTER AMS National facility (CEREGE, Aix en Provence) which is supported by the INSU/CNRS, the ANR through the "Projets thématiques d'excellence" program for the "Equipements d'excellence" ASTER-CEREGE action and IRD. The authors express their deep gratitude to Dr. Magali

Delmas and two anonymous reviewers whose detailed and interesting suggestions have helped to improve our manuscript.

References

Arnold, M., Merchel, S., Bourles, D., Braucher, R., Benedetti, L., Finkel, R.C., Aumaître, G., Gottdang, A., Klein, M., 2010. The French accelerator mass spectrometry facility ASTER: improved performance and developments. Nucl. Instrum. Methods Phys. Res. B 268, 1954-1959.

Balco, G., Stone, J. O., Lifton, N. A., Dunai, T.J., 2008. A complete and easily accessible means of calculating surface exposure ages or erosion rates from ^{10}Be and ^{26}Al measurements. Quaternary geochronology 3(3), 174-195.

Balco, G., 2011. Contributions and unrealized potential contributions of cosmogenic-nuclide exposure dating to glacier chronology, 1990–2010. Quat. Sci. Rev. 30(1-2), 3-27.

Balco, G. 2018. CRONUS-Earth online exposure age calculator v. 3. Available at: http://hess.ess.washington.edu/math/v3/v3_age_in.html (accessed _June, 2018)

Ballantyne, C.K., 2002. Paraglacial geomorphology. Quat. Sci. Rev. 21(18-19), 1935-2017.

Barrère, P., 1953. Equilibrie glacier actuel et quaternaire dans l´Ouest des Pyrénées Centrales. Revue geographique des Pyrénées et du Sud-Ouest 2, 116-134.

Batbaatar, J., Gillespie, A. R., Fink, D., Matmon, A., Fujioka, T., 2018. Asynchronous glaciations in arid continental climate. Quat. Sci. Rev. 182, 1-19.

Benson, L., Madole, R., Phillips, W., Landis, G., Thomas, T., Kubik, P., 2004. The probable importance of snow and sediment shielding on cosmogenic ages of north-central Colorado Pinedale and pre-Pinedale moraines. Quat. Sci. Rev. 23, 193-206.

Bide, J.B., 1893. Deuxième excursion dans la Sierra Nevada. Annuaire du Club Alpin Français 20, 276-305.

587 Borchers, B., Marrero, S., Balco, G., Caffee, M., Goehring, B., Lifton, N., Nishiizumi, K.,
588 Phillips, F., Schaefer, J., Stone, J., 2016. Geological calibration of spallation
589 production rates in the CRONUS-Earth project. Quat. Geochronol. 31, 188-198.
590 Braucher, R., Guillou, V., Bourles, D., Arnold, M., Aumaître, G., Keddadouche, K., Nottoli,
591 E., 2015. Preparation of ASTER in-house $^{10}Be/^{9}Be$ standard solutions. Nuclear
592 Instruments and Methods in Physics Research Section B: Beam Interactions with
593 Materials and Atoms 361, 335-340.
594 Briner, J.P., Kaufman, D.S., Manley, W.F., Finkel, R.C., Caffee, M.W., 2005. Cosmogenic
595 exposure dating of late Pleistocene moraine stabilization in Alaska. Geological
596 Society of America Bulletin 117(7-8), 1108-1120.
597 Brown, E.T., Edmond, J.M., Raisbeck, G.M., Yiou, F., Kurz, M.D., Brook, E.J., 1991.
598 Examination of surface exposure ages of Antarctic moraines using in-situ produced
599 ^{10}Be and ^{26}Al. Geochimica Cosmochimica Acta 55, 2269-2283.
600 Chenet, M., Brunstein, D., Jomelli, V., Roussel, E., Rinterknecht, V., Mokadem, F., ASTER
601 Team, 2016. ^{10}Be cosmic-ray exposure dating of moraines and rock avalanches in the
602 Upper Romanche valley (French Alps): Evidence of two glacial advances during the
603 Late Glacial/Holocene transition. Quat. Sci. Rev. 148, 209-221.
604 Chmeleff, J., von Blanckenburg, F., Kossert, K., Jakob, J., 2010. Determination of the ^{10}Be
605 half-life by multicollector ICP-MS and liquid scintillation counting. Nucl. Instrum.
606 Methods Phys. Res. B 268 (2), 192-199.
607 Clark, P.U., Dyke, A.S., Shakun, J.D., Carlson, A.E., Clark, J., Wohlfarth, B., Mitrovica, J.X.,
608 Hostetler, S.W., McCabe, A.M., 2009. The Last Glacial Maximum. Science 325, 710-
609 714.

610 Christiansen, H.H., 1998. Nivation forms and processes in unconsolidated sediments, NE
611 Greenland. Earth Surface Processes and Landforms: The Journal of the British
612 Geomorphological Group 23(8), 751-760.
613 Delmas, M., Calvet, M., Gunnell, Y., Braucher, R., Bourlès, D., 2011. Palaeogeography and
614 10Be exposure-age chronology of Middle and Late Pleistocene glacier systems in the
615 northern Pyrenees: implications for reconstructing regional palaeoclimates.
616 Palaeogeogr. Palaeoclimatol. Palaeoecol. 305, 109-122.
617 Delmas, M., 2015. The last maximum ice extent and subsequent deglaciation of the Pyrenees:
618 an overview of recent research. Cuadernos de Investigación Geográfica 41, 359-387.
619 Delunel, R., Bourlès, D.L., van der Beek, P.A., Schlunegger, F., Leya, I., Masarik, J., Paquet,
620 E., 2014. Snow shielding factors for cosmogenic nuclide dating inferred from long-
621 term neutron detector monitoring. Quat. Geochronol. 24, 16-26.
622 http://dx.doi.org/10.1016/j.quageo.2014.07.003.
623 Domínguez-Villar, D., Carrasco, R.M., Pedraza, J., Cheng, H., Edwards, R. L., Willenbring,
624 J.K., 2013. Early maximum extent of paleoglaciers from Mediterranean mountains
625 during the LPG. Scientific Reports 3, 2034.
626 Dong, G., Zhou, W., Yi, C., Zhang, L., Li, M., Fu, Y., Zhang, Q., 2017. Cosmogenic ^{10}Be
627 surface exposure dating of 'Little Ice Age' glacial events in the Mount Jaggang area,
628 central Tibet. The Holocene 27(10), 1516-1525.
629 Fernández-Fernández J.M., Palacios D., García-Ruiz, J.M., Andrés,N., Schimmelpfennig, I.,
630 Gómez-Villar, A., Santos-González, J., Álvarez-Martínez, J., Arnáez, J., Úbeda, J.,
631 Léanni, L., ASTER Team, 2017. Chronological and geomorphological investigation of
632 fossil debris-covered glaciers in relation to deglaciation processes: A case study in the
633 Sierra de La Demanda, northern Spain. Quat. Sci. Rev. 170, 232-249.
634 doi.org/10.1016/j.quascirev.2017.06.034

García-Ruiz, J.M., Martí-Bono, C., Peña-Monné, J.L., Sancho, C., Rhodes, E.J., Valero-Garcés, B., Moreno, A., 2013. Glacial and fluvial deposits in the Aragón valley, central-western Pyrenees: chronology of the Pyrenean late pleistocene glaciers. Geografiska Annaler: Series A, Physical Geography 95(1), 15-32.

García-Ruiz, J.M., Moreno, A., González-Sampériz, P., Valero-Garcés, B., Martí-Bono, C., 2010. La cronología del último ciclo glaciar en las montañas del sur de Europa. Una revisión. Cuaternario y Geomorfología 24, 35-46.

García-Ruiz, J. M., Palacios, D., González-Sampériz, P., Andrés, N., Moreno, A., Valero-Garcés, B., Gómez-Villar, A., 2016. Mountain glacier evolution in the Iberian Peninsula during the Younger Dryas. Quat. Sci. Rev. 138, 16-30.

García-Ruiz, J.M., Palacios, D., de Andrés, N., Valero-Garcés, B.L., López-Moreno, J.I., Sanjuán, Y., 2014. Holocene and 'Little Ice Age' glacial activity in the Marboré Cirque, Monte Perdido Massif, Central Spanish Pyrenees. The Holocene 24 (11), 1439-1452. doi.org/10.1177/0959683614544053

Gibbons, A.B., Megeath, J.D., Pierce, K.L., 1984. Probability of moraine survival in a succession of glacial advances. Geology 12(6), 327-330.

Gómez-Ortiz, A., Oliva, M., Salvador-Franch, F., Salvà-Catarineu, M., Plana-Castellví, J.A., 2018. The geographical interest of historical documents to interpret the scientific evolution of the glacier existing in the Veleta cirque (Sierra Nevada, Spain) during the Little Ice Age. Cuadernos de Investigación Geográfica 44 (1), 267-292.

Gómez-Ortiz, A., Palacios, D., Oliva, M., Salvador-Franch, F., Salvà-Catarineu, M., 2015. The deglaciation of Sierra Nevada (Spain): synthesis of current knowledge and new contributions. Cuadernos de Investigación Geográfica 41 (2), 409-426.

Gómez-Ortiz, A., Palacios, D., Palade, B., Vázquez-Selem, L., Salvador-Franch, F., 2012. The deglaciation of the Sierra Nevada (southern Spain). Geomorphology 159-160, 93-105.

Gómez-Ortiz, A., Palacios, D., Palade, B., Vázquez-Selem, L., Salvador-Franch, F., Tanarro, L., Oliva, M., 2013. La evolución glaciar de Sierra Nevada y la formación de glaciares rocosos. Boletín de la Asociación de Geógrafos Españoles 61, 139-162.

Gómez-Ortiz, A., Palacios, D., Ramos, M., Tanarro, L.M., Schulte, L., Salvador, F., 2001. Location of permafrost in marginal regions: Corral del Veleta, Sierra Nevada, Spain. Permafrost and Periglacial Processes 12, 93-110.

Gómez-Ortiz, A., Palacios, D., Schulte, L., Salvador-Franch, F., Plana, J.A., 2009. Evidences from historical documents of landscape evolution after Little Ice Age of a Mediterranean high mountain area, Sierra Nevada, Spain (eighteenth to twentieth centuries). Geografiska Annaler, Series A, Physical Geography 91, 279-289.

González-Trueba, J.J., Martín, R., Martínez de Pisón, E., Serrano, E., 2008. 'Little Ice Age' glaciation and current glaciers in the Iberian Peninsula. The Holocene 18, 551-568.

Gosse, J.C., Phillips, F.M., 2001. Terrestrial in situ cosmogenic nuclides: theory and application. Quat. Sci. Rev. 20, 1475-1560. http://dx.doi.org/10.1016/S0277-3791(00)00171-2.

Govin, A., Capron, E., Tzedakis, P. C., Verheyden, S., Ghaleb, B., Hillaire-Marcel, C., Blunier, T., 2015. Sequence of events from the onset to the demise of the Last Interglacial: Evaluating strengths and limitations of chronologies used in climatic archives. Quat. Sci. Rev. 129, 1-36.

Graf, A., Akçar, N., Ivy-Ochs, S., Strasky, S., Kubik, P.W., Christl, M., Schlüchter, C., 2015. Multiple advances of Alpine glaciers into the Jura Mountains in the Northwestern Switzerland. Swiss Journal of Geosciences 108(2-3), 225-238.

683 Grant, K.M., Rohling, E.J., Bar-Matthews, M., Ayalon, A., Medina-Elizalde, M., Ramsey,
684 C.B., Roberts, A.P., 2012. Rapid coupling between ice volume and polar temperature
685 over the past 150,000 years. Nature 491(7426), 744.
686 Hallet, B., Putkonen, J., 1994. Surface Dating of dynamic landforms: Young boulders on
687 aging moraines. Science 265, 937–940.
688 Häuselmann, A.D., Fleitmann, D., Cheng, H., Tabersky, D., Günther, D., Edwards, R.L.,
689 2015. Timing and nature of the penultimate deglaciation in a high alpine stalagmite
690 from Switzerland. Quat. Sci. Rev. 126, 264-275.
691 Hempel, L., 1960. Límites altitudinales geomorfológicos en Sierra Nevada. Estudios
692 Geográficos 78, 81-93.
693 Herrero, J., Polo, M.J., 2016. Evaposublimation from the snow in the Mediterranean
694 mountains of Sierra Nevada (Spain). The Cryosphere 10(6), 2981.
695 Heyman, J., Stroeven, A.P., Harbor, J.M., Caffee, M.W., 2011. Too young or too old:
696 evaluating cosmogenic exposure dating based on an analysis of compiled boulder
697 exposure ages. Earth Planet. Sci. Lett. 302, 71–80
698 Holzhauser, H., Magny, M., and Zumbühl, H.J., 2005. Glacier and lake-level variations in
699 west-central Europe over the last 3500 years: The Holocene 15, 789–801.
700 http://dx.doi.org/10.1191/0959683605hl853ra.
701 Hughes, P.D., 2014. Little Ice Age glaciers in the Mediterranean mountains. Mediterranée
702 122, 63-79.
703 Hughes, P.D., 2018. Little Ice Age glaciers and climate in the Mediterranean mountains: a
704 new analysis. Cuadernos de Investigación Geográfica 44 (1), 15-45.
705 Hughes, P.D., Woodward, J.C., Gibbard, P.L., 2007. Middle Pleistocene cold stage climates
706 in the Mediterranean: new evidence from the glacial record. Earth and Planetary
707 Science Letters 253(1-2), 50-56.

Hughes, P.D., Woodward, J.C., Van Calsteren, P.C., Thomas, L.E., 2011. The glacial history of the Dinaric Alps, Montenegro. Quat. Sci. Rev. 30(23-24), 3393-3412.

Hughes, P.D., Woodward, J.C., Gibbard, P.L., 2006a. Glacial history of the Mediterranean mountains. Progress in Physical Geography 30, 334– 364.

Hughes, P.D., Woodward, J.C., Gibbard, P.L., 2006b. Late Pleistocene glaciers and climate in the Mediterranean region. Global and Planetary Change 46, 83–98.

Heyman, J., Stroeven, A.P., Harbor, J.M., Caffee, M.W., 2011. Too young or too old: evaluating cosmogenic exposure dating based on an analysis of compiled boulder exposure ages. Earth-Planet. Sci. Lett. 302, 71–80.

Jiménez-Amat, P., Zahn, R., 2015. Offset timing of climate oscillations during the last two glacial-interglacial transitions connected with large-scale freshwater perturbation. Paleoceanography 30(6), 768-788.

Jomelli, V., Mokadem, F., Schimmelpfennig, I., Chapron, E., Rinterknecht, V., Favier, V., Swingedouw, D., 2017. Sub-Antarctic glacier extensions in the Kerguelen region (49° S, Indian Ocean) over the past 24,000 years constrained by ^{36}Cl moraine dating. Quat. Sci. Rev. 162, 128-144.

Jomelli, V., Lane, T., Favier, V., Masson-Delmotte, V., Swingedouw, D., Rinterknecht, V., Leanni, L., 2016. Paradoxical cold conditions during the medieval climate anomaly in the Western Arctic. Scientific Reports 6, 32984.

Korschinek, G., Bergmaier, A., Faestermann, T., Gerstmann, U.C., Knie, K., Rugel, G., Wallner, A., Dillmann, I., Dollinger, G., von Gostomski Lierse, Ch., Kossert, K., Maitia, M., Poutivtsev, M., Remmert, A., 2010. A new value for the half-life of 10Be by heavy-ion elastic recoil detection and liquid scintillation counting. Nucl. Instrum. Methods Phys. Res. B 268 (2), 187-191.

Kotarba A., Hercman H., Dramis, F., 2001. On the age of Campo Imperatore glaciations, Gran Sasso Massif, Central Italy. Geografia Fisica e Dinamica Quaternaria 24, 65-69.

Le Roy, M., Deline, P., Carcaillet, J., Schimmelpfennig, I., Ermini, M., ASTER Team, 2017. ^{10}Be exposure dating of the timing of Neoglacial glacier advances in the Ecrins-Pelvoux massif, southern French Alps. Quat. Sci. Rev. 178, 118-138.

Lewis, C.J., McDonald, E.V., Sancho, C., Peña, J.L., Rhodes, E.J., 2009. Climatic implications of correlated Upper Pleistocene glacial and fluvial deposits on the Cinca and Gállego rivers (NE Spain) based on OSL dating and soil stratigraphy. Global and Planetary Change 67, 141-152.

Lhenaff, R., 1977. Recherches géomorphologiques sur les Cordillères Bétiques centro-occidentales (Espagne). PhD thesis, University of Lille.

Li, Y., Li, Y., Harbor, J., Liu, G., Yi, C., Caffee, M.W., 2016. Cosmogenic ^{10}Be constraints on Little Ice Age glacial advances in the eastern Tian Shan, China. Quat. Sci. Rev. 138, 105-118.

Licciardi, J.M., Schaefer, J.M., Taggart, J.R., Lund, D.C., 2009. Holocene glacier fluctuations in the Peruvian Andes indicate northern climate linkages. Science 325, 1677–1679. http://dx.doi.org/10.1126/science.1175010.

Lifton, N., Sato, T., Dunai, T.J., 2014. Scaling in situ cosmogenic nuclide production rates using analytical approximations to atmospheric cosmic-ray fluxes. Earth Planet. Sci. Lett. 386, 149-160.

Martin, L., Blard, P.-H., Balco, G., Lave, J., Delunel, R., Lifton, N., Laurent, V., 2017. The CREp program and the ICE-D production rate calibration database: a fully parameterizable and updated online tool to compute cosmic-ray exposure ages. Quat. Geochronol. 38, 25-49.

Martini, M.A., Kaplan, M.R., Strelin, J.A., Astini, R.A., Schaefer, J.M., Caffee, M.W., Schwartz, R., 2017. Late Pleistocene glacial fluctuations in Cordillera Oriental, subtropical Andes. Quat. Sci. Rev. 171, 245-259.

Martrat, B., Jimenez-Amat, P., Zahn, R., Grimalt, J.O., 2014. Similarities and dissimilarities between the last two deglaciations and interglaciations in the North Atlantic region. Quat. Sci. Rev. 99, 122-134.

Mayewski, P.A., Rohling, E.E., Stager, C., Karlén, W., Maasch, K.A., Meeker, L.D., Meyerson, E.A., Gasse, F., Van Kreveld, S., Holmgren, K., Leethrop, J., Rosqvist, G., Rack, F., Staubwasser, M., Schneider, R.R., Steig, E.J., 2004. Holocene climate variability. Quaternary Research 62 (3), 243-255.

Merchel, S., Herpers, U., 1999. An update on radiochemical separation techniques for the determination of longlived radionuclides via Accelerator Mass Spectrometry. Radiochim. Acta 84, 215-219.

Messerli, B., 1965. Beiträge zur Geomorphologie der Sierra Nevada (Andalusien). Juris Verlag. Zürich.

Moseley, G.E., Spötl, C., Cheng, H., Boch, R., Min, A., Edwards, R.L., 2015. Termination-II interstadial/stadial climate change recorded in two stalagmites from the north European Alps. Quat. Sci. Rev. 127, 229-239.

Nussbaum, F., 1949. Sur les traces des glaciers quaternaires dans la région de l'Aragón. Pirineos 13-14, 497-518.

Obermaier, H., 1914. Estudio de los glaciares de los Picos de Europa. Museo Nacional de Ciencias Naturales, Madrid.

Obermaier, H., 1916. Los glaciares cuaternarios de Sierra Nevada. Trabajos del Museo Nacional de Ciencias Naturales (Geología) 17, 1-68.

780 Obermaier, H., Carandell, J., 1917. Los glaciares cuaternarios de la Sierra de Guadarrama.
781 Trabajos del Museo Nacional de Ciencias Naturales, 19, 1-92.
782 Oliva, M., Gómez-Ortiz, A. 2012. Late Holocene environmental dynamics and climate
783 variability in a Mediterranean high mountain environment (Sierra Nevada, Spain)
784 inferred from lake sediments and historical sources. The Holocene 22 (8), 915-927.
785 Oliva, M., Gómez-Ortiz, A., Palacios, D., Salvador-Franch, F., Salvà-Catarineu, M., 2014.
786 Environmental evolution in Sierra Nevada (South Spain) since the LPG based on
787 multi-proxy records. Quaternary International 353, 195-209.
788 Oliva, M., Ruiz-Fernández, J. 2015. Coupling patterns between paraglacial and permafrost
789 degradation responses in Antarctica. Earth Surface Processes and Landforms 40 (9),
790 1227-1238.
791 Oliva, M., Ruiz-Fernández, J., Barriendos, M., Benito, G., Cuadrat, J.M., García-Ruiz, J.M.,
792 Giralt, S., Gómez-Ortiz, A., Hernández, A., López-Costas, O., López-Moreno, J.I.,
793 López-Sáez, J.A., Martínez-Cortizas, A., Moreno, A., Prohom, M., Saz, M.A., Serrano,
794 E., Tejedor, E., Trigo, R., Valero-Garcés, B., Vicente-Serrano, S., 2018a. The Little Ice
795 Age in Iberian mountains. Earth-Science Reviews 177, 175-208.
796 Oliva, M., Žebre, M., Guglielmin, M., Çiner, A., Vieira, G., Bodin, X., Andrés, N., Colucci,
797 R.R., García-Hernández, C., Hughes, P., Mora, C., Nofre, J., Palacios, D., Pérez-
798 Alberti, A., Ribolini, A., Ruiz-Fernández, J., Sarıkaya, M.A., Serrano, E., Urdea, P.,
799 Valcárcel, M., Woodward, J., Yıldırım, C., 2018b. Permafrost conditions in the
800 Mediterranean region since the LPG. Earth-Science Reviews 185, 397-436.
801 Oliva, M., Serrano, E., Gómez-Ortiz, A., González Amuchastegui, M.J., Nieuwendam, A.,
802 Palacios, D., Pellitero-Ondicol, R., Pérez-Alberti, A., Ruiz-Fernández, J., Valcárcel,
803 M., Vieira, G., 2016b. Spatial and temporal variability of periglaciation of the Iberian
804 Peninsula. Quat. Sci. Rev., 137, 176-199.

805 Oliva, M., Gómez-Ortiz, A., Salvador-Franch, F., Salvà-Catarineu, M., Ramos, M., Palacios,
806 D., Tanarro, L., Pereira, P., Ruiz-Fernández, J., 2016a. Inexistence of permafrost at the
807 top of Veleta peak (Sierra Nevada, Spain). Science of the Total Environment 550, 484-
808 494.
809 Oppo, D.W., J.F. McManus, Cullen, J. L., 2006. Evolution and demise of the last interglacial
810 warmth in the subpolar North Atlantic, Quat. Sci. Rev. 25, 3268–3277.
811 Osborn, G., 1986. Lateral-moraine stratigraphy and neoglacial history of Bugaboo Glacier,
812 British Columbia. Quaternary Research 26(2), 171-178.
813 Palacios, D., de Andrés, N., Luengo, E., 2003. Distribution and effectiveness of nivation in
814 Mediterranean mountains: Peñalara (Spain). Geomorphology 54(3-4), 157-178.
815 Palacios, D., Andrés, N., Gòmez-Ortiz, A., García-Ruiz, J.M., 2017a. Evidence of glacial
816 activity during the Oldest Dryas in the Mountain of Spain. In: Hughes, P. and
817 Woodward, J. (Eds.) Quaternary glaciation in the Mediterranean Mountains. Geological
818 Society of London, Special Publication, 433(1), 87-110. doi.org/10.1144/SP433.10
819 Palacios, D., García-Ruiz, J.M., Andrés, N., Schimmelpfennig, I., Campos, N. Leanni, L.,
820 ASTER Team, 2017b. Deglaciation in the central Pyrenees during the Pleistocene-
821 Holocene transition: Timing and geomorphological significance. Quat. Sci. Rev. 162,
822 111-127. doi.org/10.1016/j.quascirev. 2017.03.007
823 Palacios, D., Gómez-Ortiz, Andres, N., Salvador, F., Oliva, M., 2016. A Timing and new
824 geomorphologic evidence of the last deglaciation stages in Sierra Nevada (southern
825 Spain) Quat. Sci. Rev. 150, 110-129 doi.org/10.1016/j.quascirev.2016.08.012
826 Pallàs, R., Rodes, A., Braucher, R., Bourles, D., Delmas, M., Calvet, M., Gunnell, Y. 2010.
827 Small, isolated glacial catchments as priority target for cosmogenic surface dating of
828 Pleistocene climate fluctuations, SE Pyrenees. Geology 38, 891-894.

Palma, P., Oliva, M., García-Hernández, C., Gómez Ortiz, A., Ruiz-Fernández, J., Salvador-Franch, F., Catarineu, M., 2017. Spatial characterization of glacial and periglacial landforms in the highlands of Sierra Nevada (Spain). Sci. Total Environ. 584–585, 1256–1267. https://doi.org/10.1016/j.scitotenv.2017.01.196

Penck, A., 1883. La période glaciaire dans les Pyrénées. Bulletin de la Société d'Histoire Naturelle de Toulouse 19, 105-200.

Penck, A., 1897. Die Picos de Europa und das kantabrische Gebirge. Geographische Zeitschrift, 278-281.

Putkonen, J., Swanson, T., 2003. Accuracy of cosmogenic ages for moraines. Quaternary Research. 59, 255–261.

Putkonen, J., Connolly, J., Orloff, T., 2008. Landscape evolution degrades the geologic signature of past glaciations. Geomorphology 97, 208-217.

Putkonen, J., O'Neal, M., 2006. Degradation of unconsolidated Quaternary landforms in the western North America. Geomorphology 75, 408-419.

Quelle, O., 1908. Beiträge zur Kenntnis der spanischen Sierra Nevada. Friedrich-Wilheilms Universität, Berlin.

Rodríguez-Rodríguez, L., Jiménez-Sánchez, M., Domínguez-Cuesta, M.J., Rinterknecht, V., Pallàs, R., Bourlès, D., 2016. Chronology of glaciations in the Cantabrian Mountains (NW Iberia) during the Last Glacial Cycle based on in situ-produced ^{10}Be. Quat. Sci. Rev. 138, 31-48.

Rodríguez-Rodríguez, L., Jiménez-Sánchez, M., Domínguez-Cuesta, M.J., Rinterknecht, V., Pallàs, R., Aumaître, G., Bourlès, D.L., Keddadouche, K., 2017. Timing of last deglaciation in the Cantabrian Mountains (Iberian Peninsula; North Atlantic Region) based on in situ-produced ^{10}Be exposure dating. Quat. Sci. Rev. 171, 166–181. https://doi.org/10.1016/j.quascirev.2017.07.012

Rohling, E.J., Hibbert, F.D., Williams, F.H., Grant, K.M., Marino, G., Foster, G. L., Webster, J.M., 2017. Differences between the last two glacial maxima and implications for ice-sheet, $\delta^{18}O$, and sea-level reconstructions. Quat. Sci. Rev. 176, 1-28.

Sánchez-Gómez, S., 1990. Aplicación del estudio de suelos a la dinámica de la cuenca del río Lanjarón. Relación suelos-geomorfología. PhD thesis, University of Granada.

Sanz de Galdeano, C., López-Garrido, A.C., 1999. Nature and impact of the Neotectonic deformation in the western Sierra Nevada (Spain). Geomorphology 30 (3), 259-272.

Schaefer, J.M., Oberholzer, P., Zhao, Z., Ivy-Ochs, S., Wieler, R., Baur, H., Schlüchter, C. 2008. Cosmogenic beryllium-10 and neon-21 dating of late Pleistocene glaciations in Nyalam, monsoonal Himalayas. Quat. Sci. Rev. 27(3-4), 295-311.

Schaefer, J.M., Denton, G.H., Kaplan, M., Putnam, A., Finkel, R.C., Barrell, D.J.A., Andersen, B.G., Schwartz, R., Mackintosh, A., Chinn, T., Schlüchter, C., 2009. High frequency Holocene glacier fluctuations in New Zealand differ from the northern signature. Science 324, 622–625. http://dx.doi.org/10.1126/science.1169312.

Schildgen, T.F., Phillips, W.M., Purves, R.S., 2005. Simulation of snow shielding corrections for cosmogenic nuclide surface exposure studies. Geomorphology 64, 67–85.

Schimmelpfennig, I., Schaefer, J.M., Akçar, N., Ivy-Ochs, S., Finkel, R.C., Schlüchter, C., 2012. Holocene glacier culminations in the Western Alps and their hemispheric relevance. Geology 40, 891–894. doi:10.1130/G33169.1

Schimmelpfennig, I., Schaefer, J.M., Akçar, N., Koffman, T., Ivy-Ochs, S., Schwartz, R., Finkel, R.C., Zimmerman, S., Schlüchter, C., 2014. A chronology of Holocene and Little Ice Age glacier culminations of the Steingletscher, Central Alps, Switzerland, based on high-sensitivity beryllium-10 moraine dating. Earth and Planetary Science Letters 393, 220-230.

878 Styllas, M.N., Schimmelpfennig, I., Benedetti, L., Ghilardi, M., ASTER Team, 2018. Late-
879 glacial and Holocene history of the northeast Mediterranean mountains-New insights
880 from in situ-produced 36Cl-based cosmic ray exposure dating of paleo-glacier
881 deposits on Mount Olympus, Greece. Quat. Sci. Rev. 193, 244-265.
882 Uppala, S.M., Kållberg, P., Simmons, A., Andrae, U., Bechtold, V., Fiorino, M., Gibson, J.,
883 Woollen, J., 2005. The ERA-40 reanalysis. Q.J.R. Meteorological Soc. 131, 2961-
884 3012.
885 Vidal-Romaní, J.R., Fernández-Mosquera, D., Marti, K., 2015. The glaciation of Serra de
886 Queixa-Invernadoiro and Serra do Gerês-Xurés, NW Iberia. A critical review and a
887 cosmogenic nuclide (^{10}Be and ^{21}Ne) chronology. Cadernos do Laboratorio Xeolóxico
888 de Laxe 38, 25-44.
889 Villa, E., Stoll, H., Farias, P., Adrados, L., Edwards, R.L., Cheng, H., 2013. Age and
890 significance of the Quaternary cemented deposits of the Duje Valley (Picos de
891 Europa, Northern Spain). Quaternary Research 79, 1-5.
892 Young, N.E., Schweinsberg, A.D., Briner, J.P., Schaefer, J.M., 2015. Glacier maxima in
893 Baffin Bay during the Medieval Warm Period coeval with Norse settlement. Science
894 advances 1(11), e1500806.
895 Zreda, M.G., Phillips, F.M., 1995. Insights into alpine moraine development from cosmogenic
896 ^{36}Cl buildup dating. Geomorphology 14(2), 149-156.
897 Zreda, M.G., Phillips, F.M., 1994. Cosmogenic ^{36}Cl accumulation in unstable landforms.
898 Water Resources Research 30, 3127–3136.
899 Zweck, C., Zreda, M., Desilets, D., 2013. Snow shielding factors for cosmogenic nuclide
900 dating inferred from Monte Carlo neutron transport simulations. Earth Planet Sci.
901 Lett. 379, 64-71. http://dx.doi.org/10.1016/j.epsl.2013.07.023.
902

903 **Figure captions**

904

905 Figure 1. Location of the case study area, Sierra Nevada, in the south of the Iberian Peninsula.

906 Figure 2. Geomorphological map of the Naute valley and location of samples. We show CRE
907 ka ages from this work (NAUT samples) together with those from Palacios et al. (2016).

908 Figure 3. Results of the Naute moraine samples of this work, together with pictures of some
909 of the sampled boulders and CRE data (including data from Palacios et al. (2016)). (A)
910 Penultimate glaciation moraine (source: Google Earth imagery), (B) Picture of the sampled
911 NAUT-4 boulder, (C) Panoramic view of the penultimate glaciation moraine next to the last
912 glaciation moraine.

913 Figure 4. Geomorphological sketch of the two moraines existing in the lower part of the
914 Naute valley, together with the location of the CRE Sampling Boulder (CSB).

915 Figure 5. Geomorphological map of the Veleta cirque and sample location. We show CRE
916 ages from this work (SN samples) together with those from Palacios et al. (2016).

917 Figure 6. (A) Schematic transect of the Veleta cirque including the different landforms
918 existing across the cirque floor, and (B) Sketch showing the geomorphological approach used
919 in the selection of samples in the Veleta cirque.

920 Figure 7. (A) Photograph of Corral of the Veleta cirque from the West in September, 2016.
921 (B) Drawing according to the vision of Bide (1893), where the glacier seems still to cover its
922 maximum extension in 19th century.

923 Figure 8. (A) Veleta cirque with its 19th century moraine (source: Google Earth), (B) Vertical
924 view of the Veleta cirque floor from the Veleta peak, (C) Sampled boulder for SN-11-2, and
925 (D) Sampled boulder for SN-11-3.

926 Figure 9. Sketch representing the erosion processes affecting a moraine: (A) Intense mass
927 movements and erosion reshaping the main ridge during the paraglacial stage, (B)
928 Stabilization phase of a moraine at the end of paraglacial phase, and (C) Mature stage of an
929 old moraine after a long period of erosion.

930 **Table captions**

931 Table 1. Current knowledge of Quaternary glacial stages in Sierra Nevada.

932 Table 2. Field data and characteristics of sampled boulders dated with ^{10}Be in Sierra Nevada
933 (*boulders are covered by snow thickness of 30 to 130 cm during 8 months per year). See text
934 for details.

935 Table 3. Analytical data and ^{10}Be sample exposure ages.

Table

Table 1. Current knowledge of Quaternary glacial stages in Sierra Nevada.

Stage	Chronology	Processes and landforms
Pre-Last Glaciation	Unknown	Possible existence of eroded moraines from glaciations occurred before the Last Glaciation as well as glacio-fluvial sediments distributed at lower elevations than moraines formed during the Last Glaciation (Hempel, 1960; Messerli, 1965; Lhenaff, 1977; Sánchez-Gómez, 1990).
Last Glaciation (Maximum Ice Extent; MIE)	Two glacial advances at ca. 32-30 ka and 20-19 ka	Development of alpine valleys at elevations between 2000 and 2500 m in northern and southern slopes, respectively (Gómez-Ortiz et al., 2012, 2013, 2015; Oliva et al., 2014; Palacios et al., 2016). The glaciated environment during the MIE encompassed 105 km^2 (Palma et al., 2017).
Deglaciation	Two glacial advances during the Oldest Dryas (OD) at ca. 17 ka and Younger Dryas (YD) at ca. 13-12 ka	Glacial retreat at ca. 19 ka followed by two phases of glacial development until the Holocene, mainly in the highest valleys from the northern slope of the massif (Gómez-Ortiz et al., 2012, 2013; Oliva et al., 2012, 2014; Palacios et al., 2016).
Holocene	Glacial retreat until the Early Holocene at ca. 10-9 ka	The glaciers formed during the YD finally melted and paraglacial activity favoured the development of rock glaciers in these areas (Gómez-Ortiz et al., 2012, 2013; Oliva et al., 2016b; Palacios et al., 2016).
	Three stages with formation of glaciers occurred during the Late Holocene at ca. 2.8-2.7, 1.4-1.2 ka cal BP and LIA	Lake sediments suggest the development of a small glacier in the Mulhacén cirque, which is reflected in several moraine ridges distributed across the cirque floor (Oliva and Gómez-Ortiz, 2012; Oliva et al., 2016a).
Little Ice Age (LIA)	From 1440 to 1710 AD a glacier existed in the Mulhacén cirque, and another glacier developed in the Corral de Veleta cirque until the mid-20th century	In the highest northern cirques between Mulhacén and Veleta peaks, historical sources and geomorphic evidence (i.e. moraines) shows evidence of the existence of several small glaciers that gradually disappeared during the 19th and 20th centuries (Gómez-Ortiz et al., 2001, 2009, 2018; Oliva and Gómez-Ortiz, 2012; Oliva et al., 2018a).

Table

Table 2. Field data and characteristics of sampled boulders dated with ^{10}Be in Sierra Nevada (*boulders are covered by snow thickness of 30 to 130 cm during 8 months per year). See text for details.

Sample	Latitude (ºN)	Longitude (ºW)	Elevation (m a.s.l.)	Thickness (cm)	Topographic shielding factor	Snow shielding factor
NAUT-1	37.0196111	3.33047222	2164	1.5	0.97832	
NAUT-2	37.0201111	3.33036111	2179	1.5	0.98414	
NAUT-3	37.0212500	3.32977778	2211	1.5	0.98221	
NAUT-4	37.0225556	3.32866667	2263	3.0	0.97817	
*SN-11-1	37.0595833	3.36569444	3076	2.5	0.80979	0.70067
*SN-11-2	37.0605833	3.36747222	3061	2.0	0.80979	0.70067
*SN-11-3	37.0606944	3.36897222	3095	2.0	0.80979	0.70067

Table

Table 3. Analytical data and ^{10}Be sample exposure ages

Sample	Quartz (g)	^{9}Be carrier solution (mg) [a]	^{10}Be/^{9}Be (x10^{13}) [b]	[^{10}Be] (x10^{3} at.g^{-1})	^{10}Be age (CREp [c]) (ka)	^{10}Be age (C-E [d]) (ka)	^{10}Be age (CREp [c]) (ka) With snow shielding factor	^{10}Be age (C-E [d]) (ka) With snow shielding factor
NAUT-1	18.32	98.9	23.3 ± 1.0	2530 ± 110	134.8 ± 10 (6.2)	130.4 ± 10 (6.1)		
NAUT-2	21.98	100.2	11.2 ± 0.58	1030 ± 53	53.7 ± 4.3 (2.9)	54.5 ± 4.3 (2.9)		
NAUT-3	22.53	100.5	9.62 ± 0.55	868 ± 50	43.8 ± 3.2 (2.3)	43.0 ± 3.6 (2.5)		
NAUT-4	22.62	100.7	28.6 ± 1.2	2580 ± 110	129.2 ± 8.9 (5.4)	125.4 ± 9.4 (5.5)		
SN-11-1	30.91	100.9	0.127 ±0.052	8.4 ± 3.5	0.31 ± 0.10 (0.10)	0.28 ± 0.11 (0.11)	0.34 ± 0.12 (0.12)	0.32 ± 0.13 (0.13)
SN-11-2	32.79	100.7	0.285 ± 0.086	17.7 ± 5.3	0.60 ± 0.22 (0.21)	0.59 ± 0.20 (0.18)	0.72 ± 0.28 (0.27)	0.71 ± 0.22 (0.22)
SN-11-3	31.39	101.0	0.159 ± 0.050	10.3 ± 3.3	0.36 ± 0.09 (0.09)	0.35 ± 0.11 (0.10)	0.40 ± 0.11 (0.11)	0.38 ± 0.12 (0.12)
Blank		99.4	0.0450 ± 0.013					

[a] Carrier has a concentration of 3025 µg ^{9}Be/g.
[b] Sample ^{10}Be/^{9}Be ratios corrected for batch-specific analytical blank ratio of (4.5 ± 1.3) x 10^{-15}.
[c] ^{10}Be ages calculated with the online CREp exposure age calculator (Martin et al., 2017). 1sigma errors include analytical and production rate uncertainties; analytical errors shown in brackets.
[d] ^{10}Be ages calculated with the online exposure age calculator formerly known as the CRONUS-Earth online exposure age calculator version 3 (Balco et al., 2008). 1sigma errors include analytical and production rate uncertainties; analytical errors shown in brackets.

Figure (Color)

Click here to download high resolution image

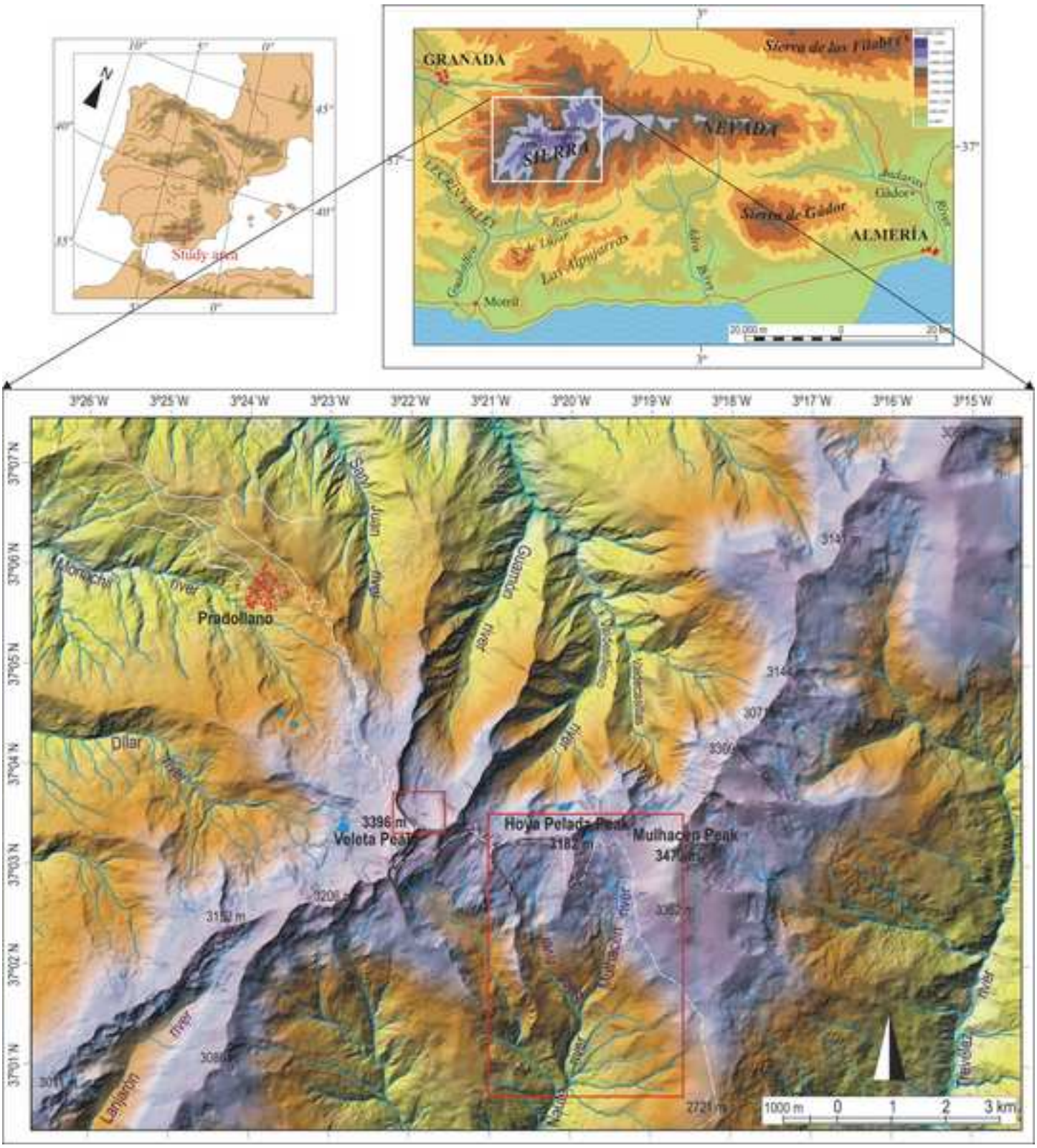

Figure (Color)

Click here to download high resolution image

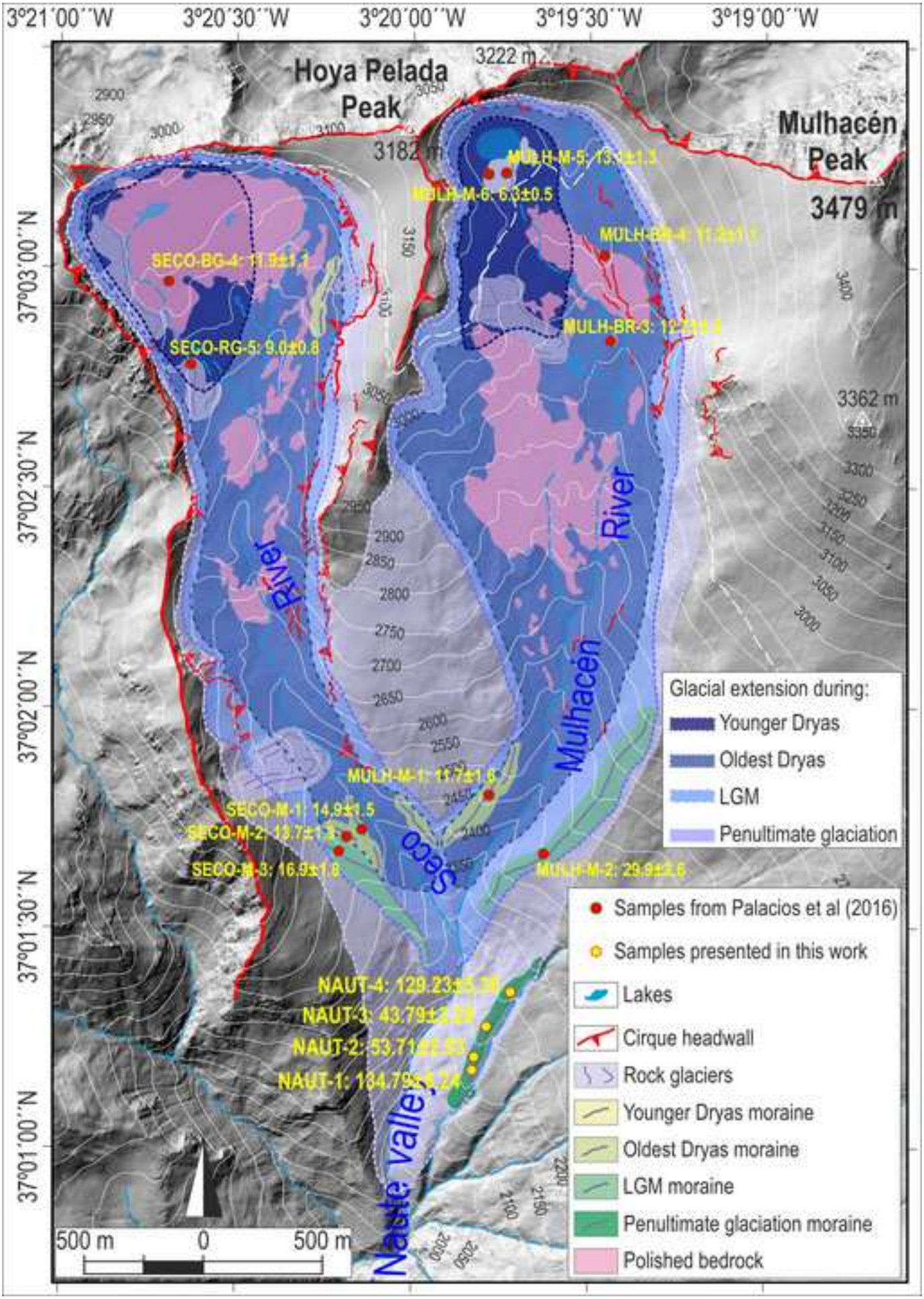

Figure (Color)

Click here to download high resolution image

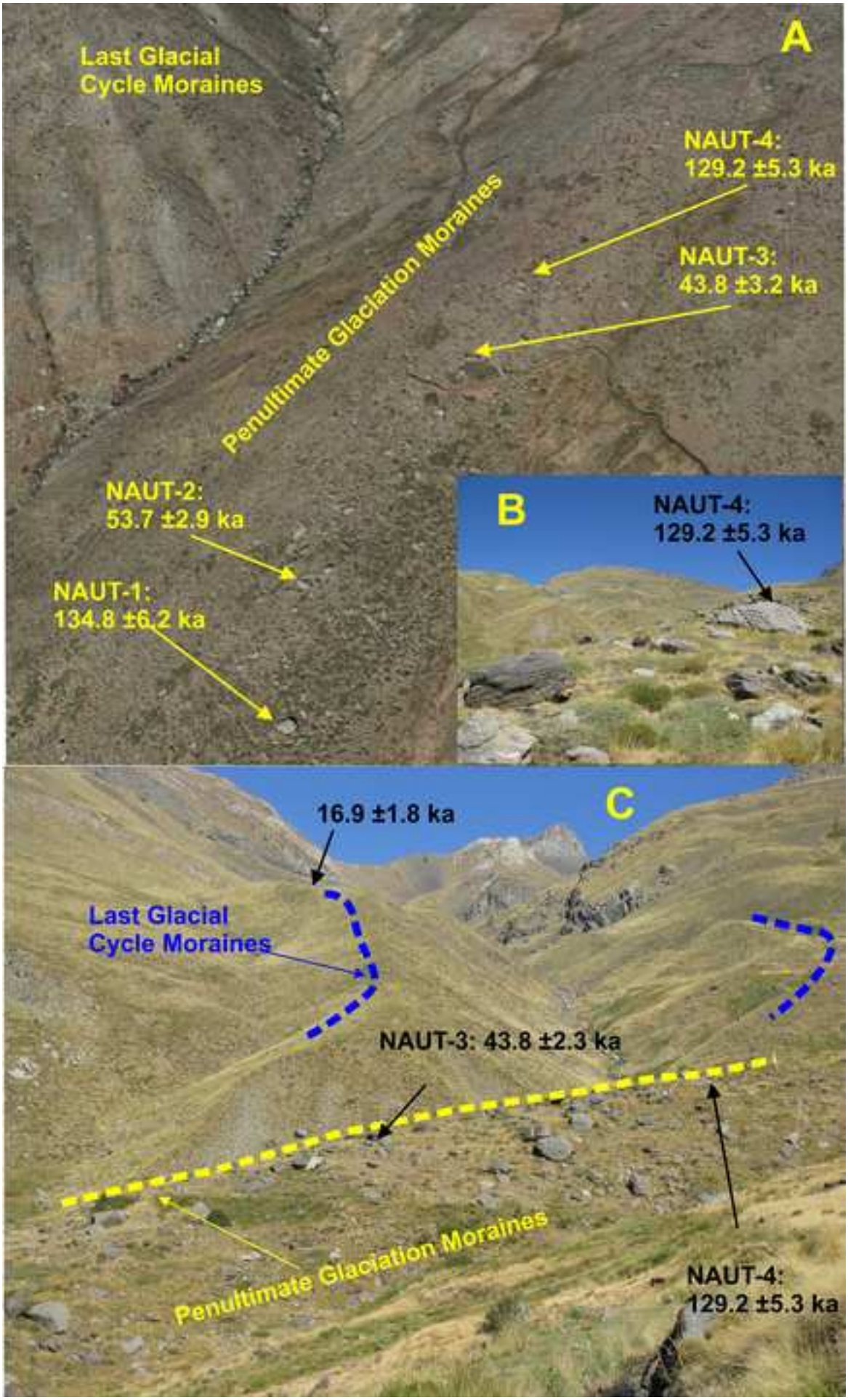

Figure (Color)
Click here to download high resolution image

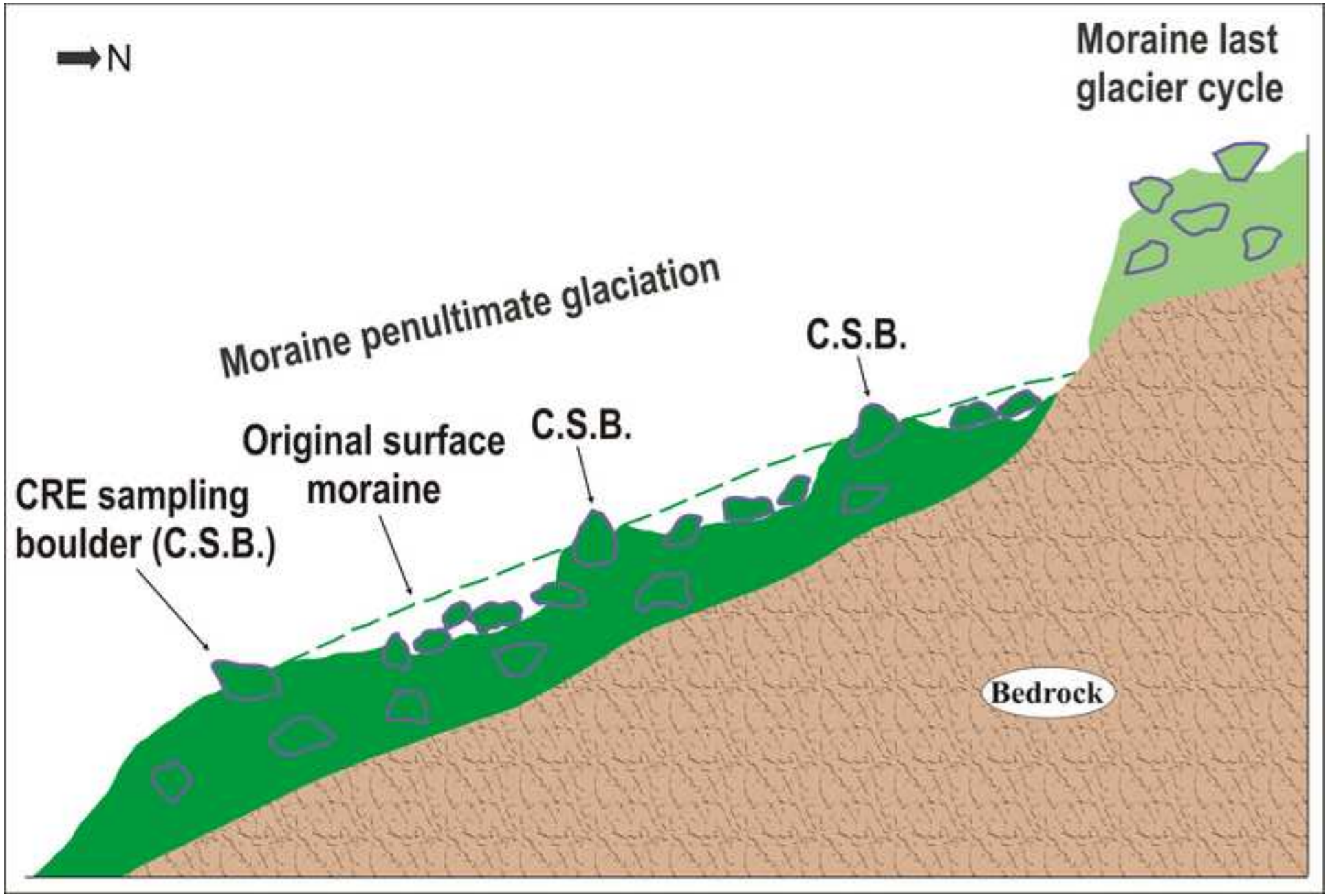

Figure (Color)

Click here to download high resolution image

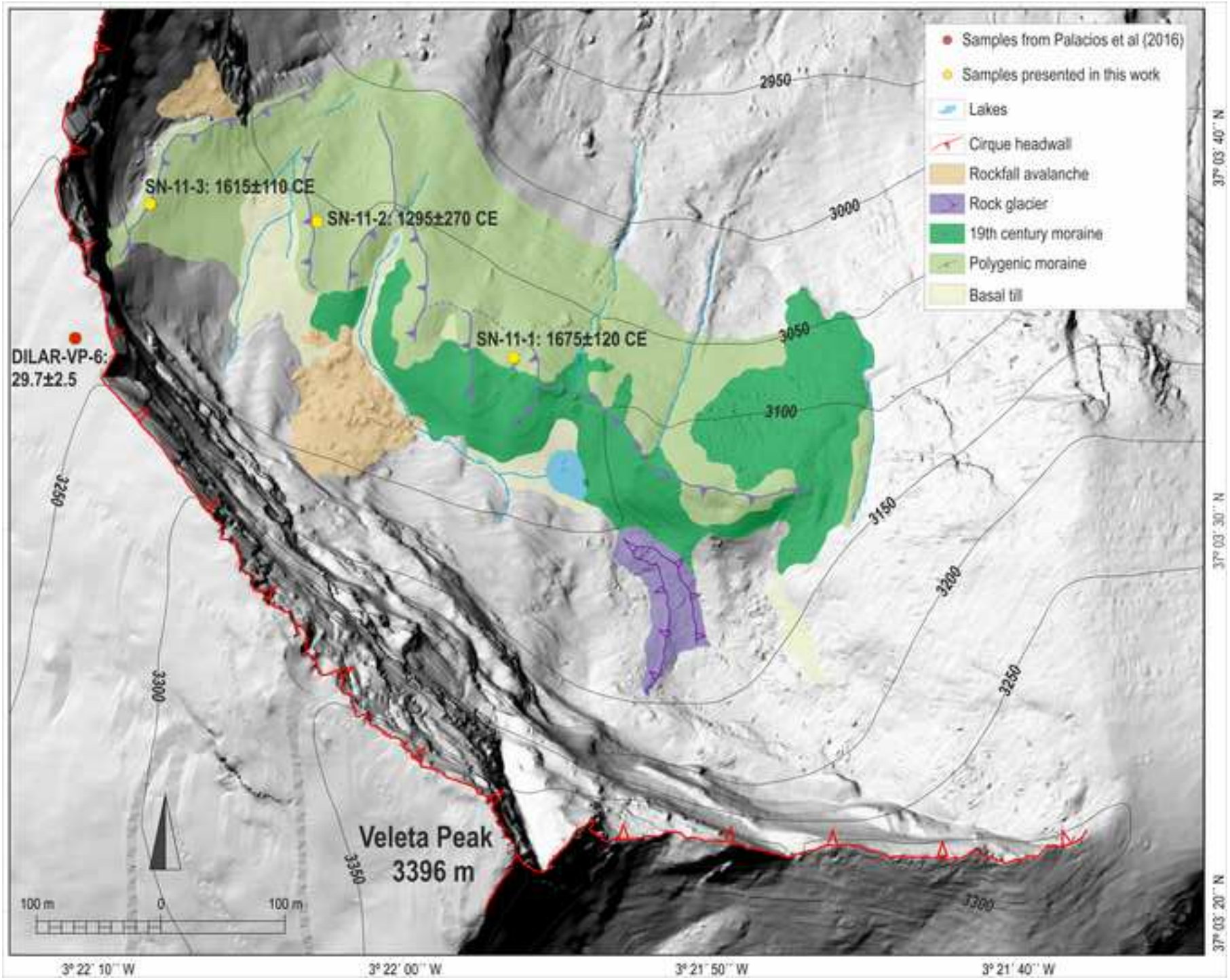

Figure (Color)
Click here to download high resolution image

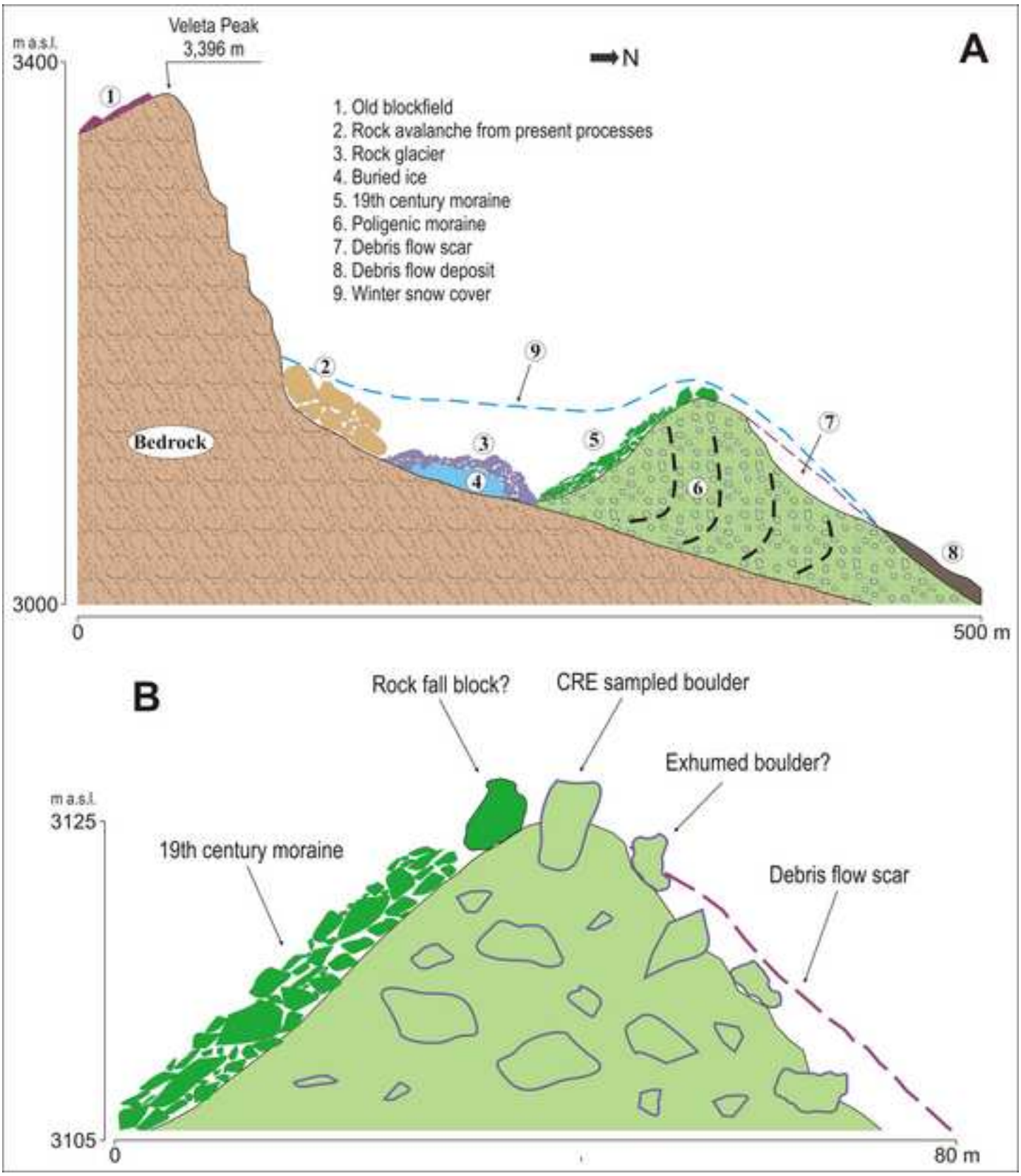

Figure (Color)
Click here to download high resolution image

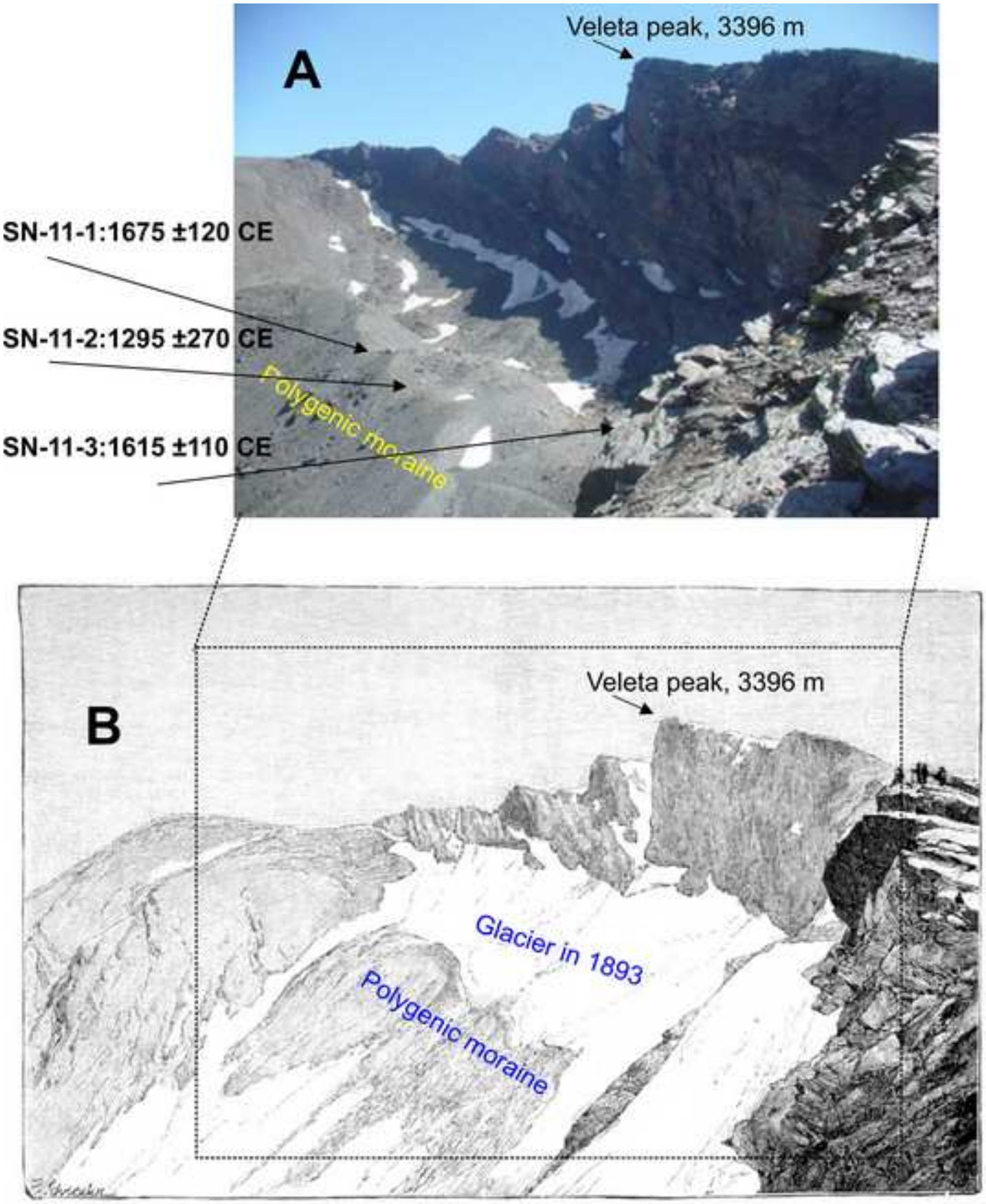

Figure (Color)

Click here to download high resolution image

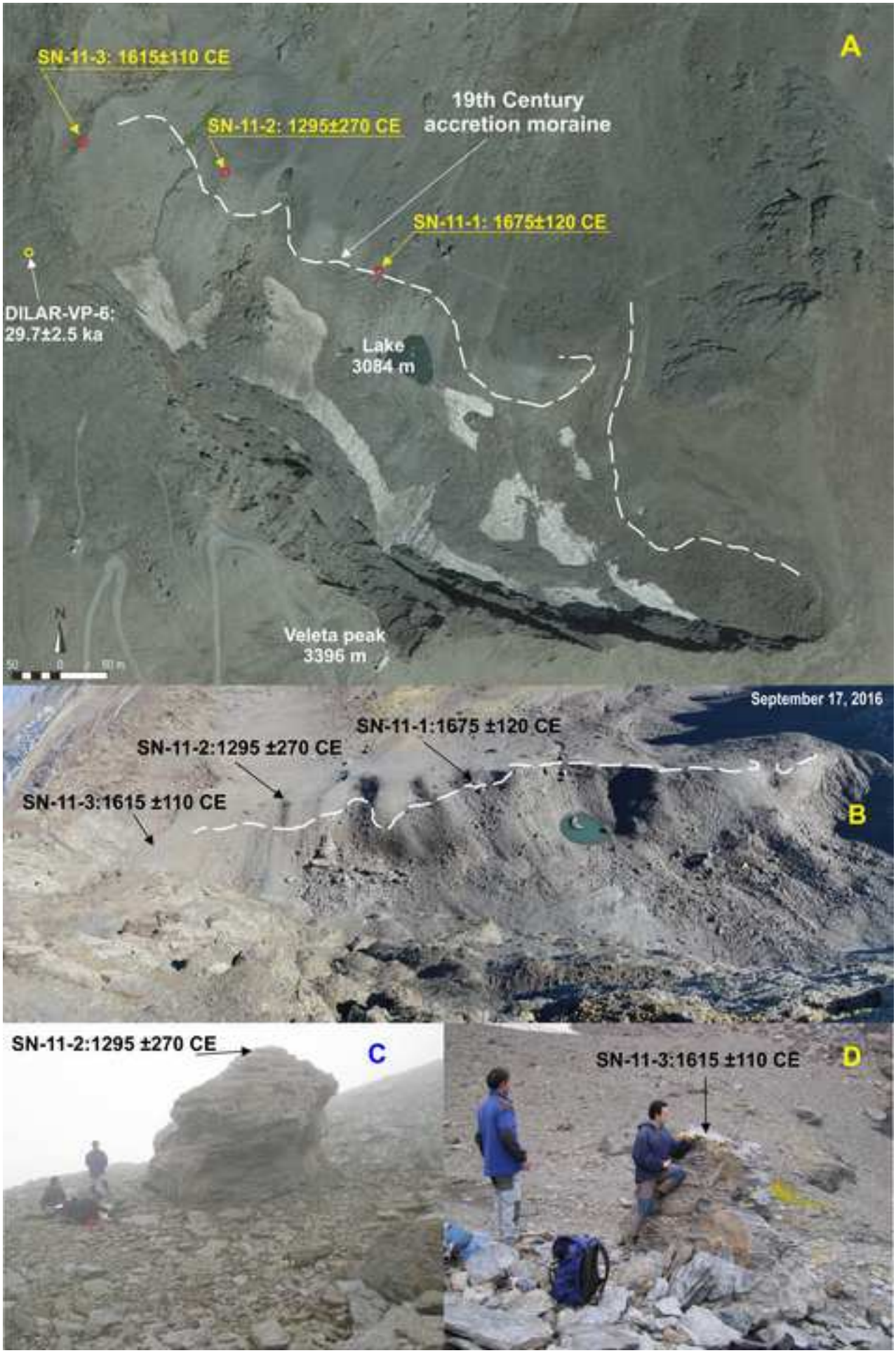

Figure (Color)
Click here to download high resolution image

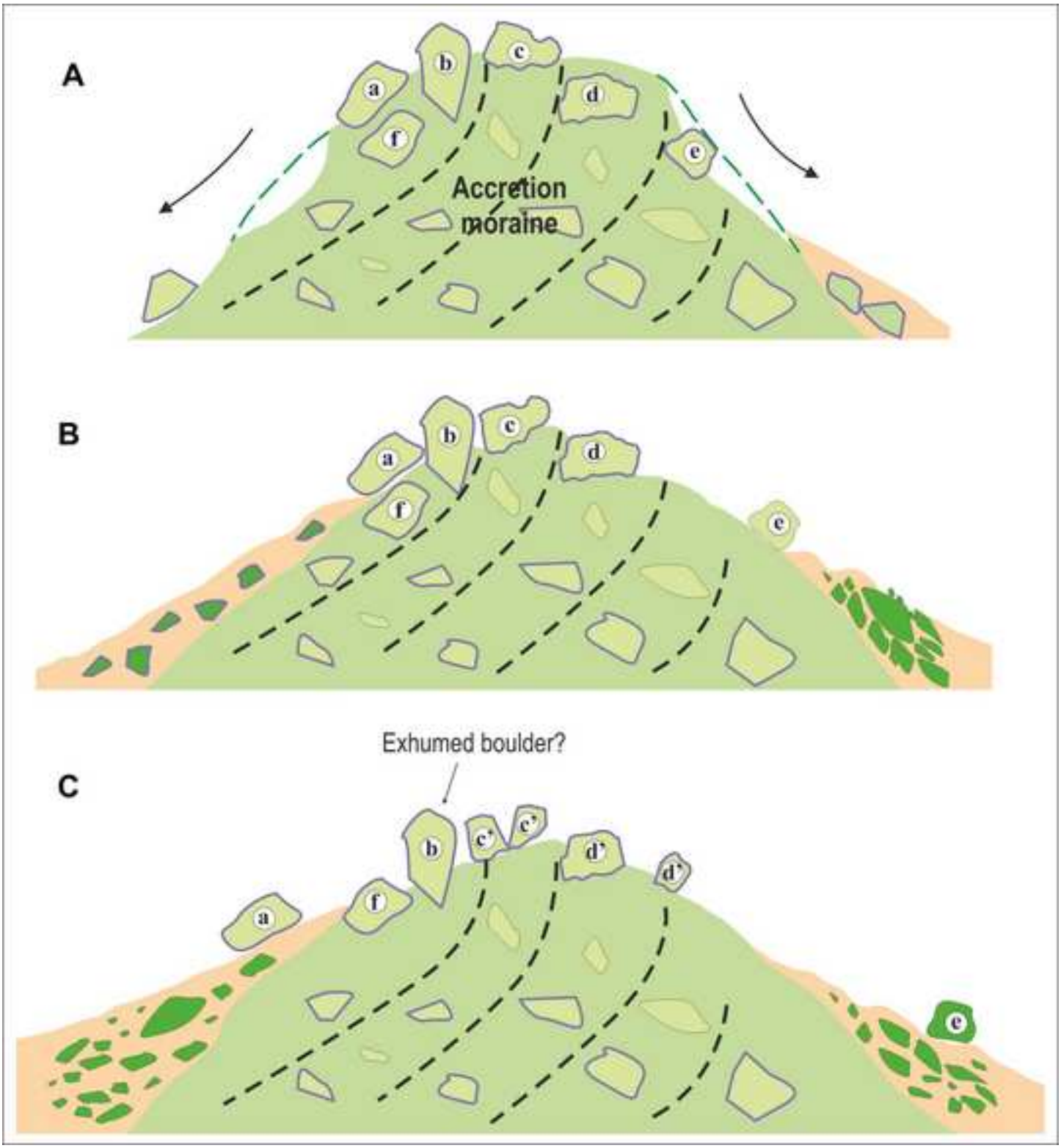

Figure (Greyscale)

Click here to download high resolution image

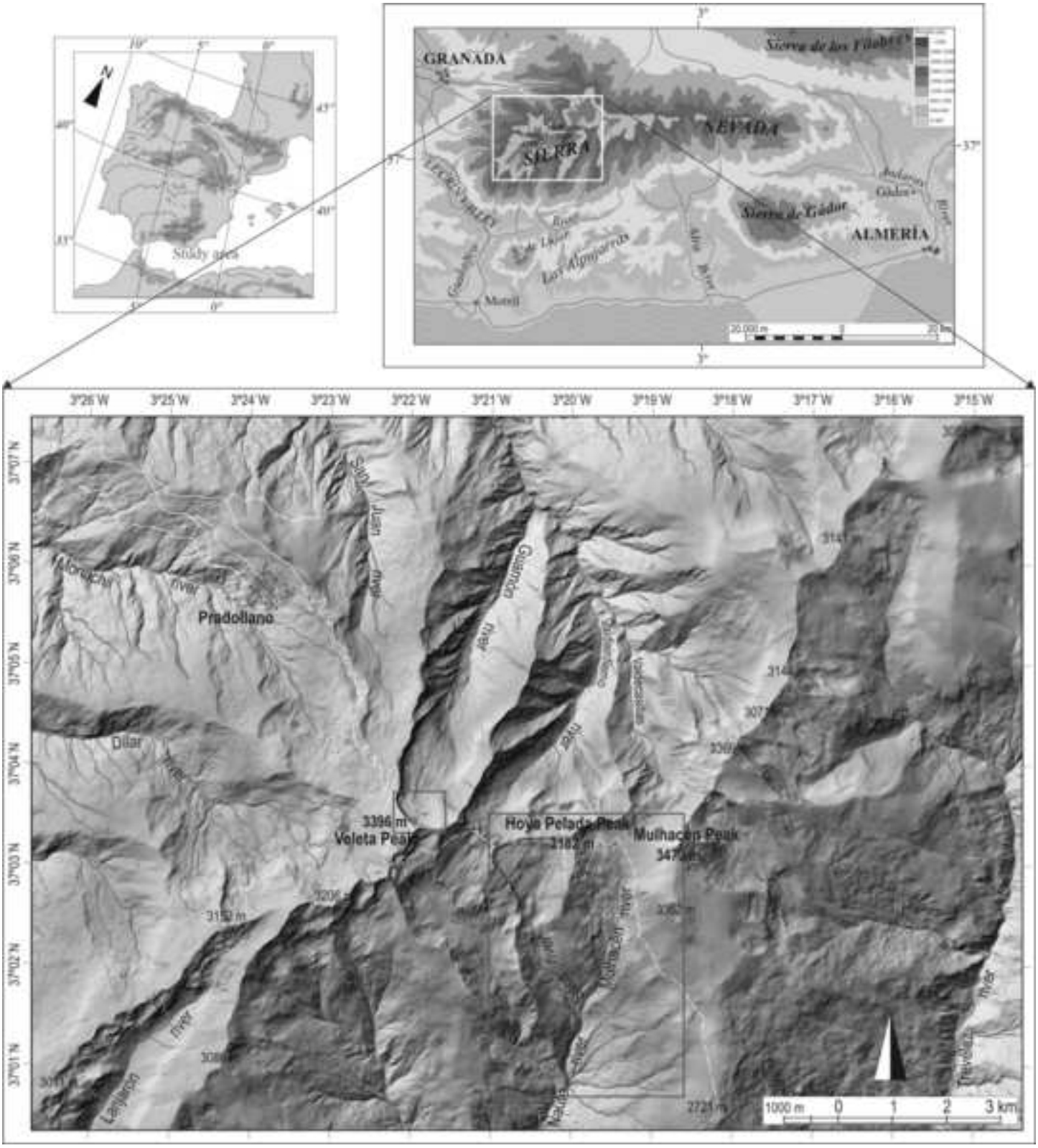

Figure (Greyscale)

Click here to download high resolution image

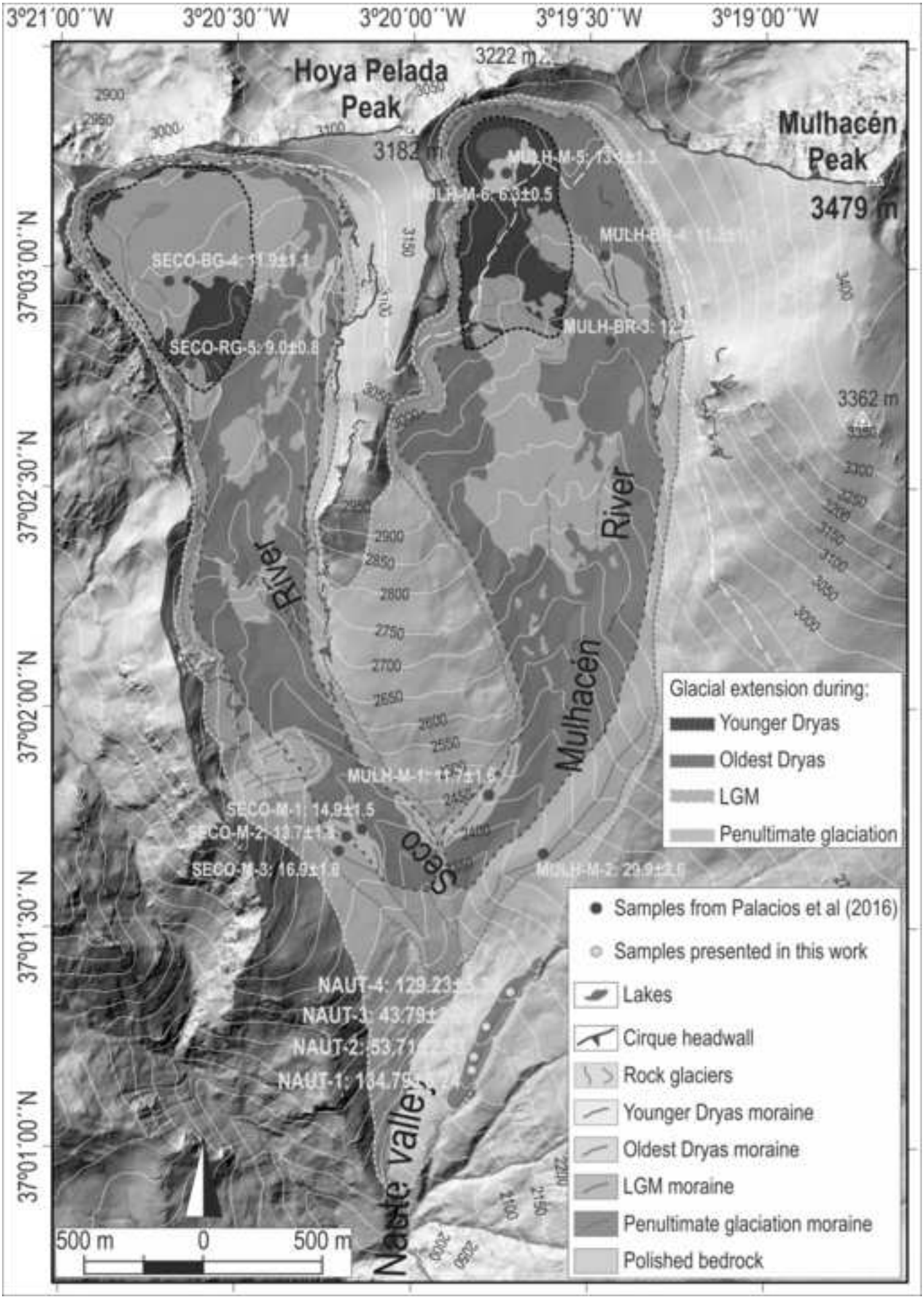

Figure (Greyscale)
Click here to download high resolution image

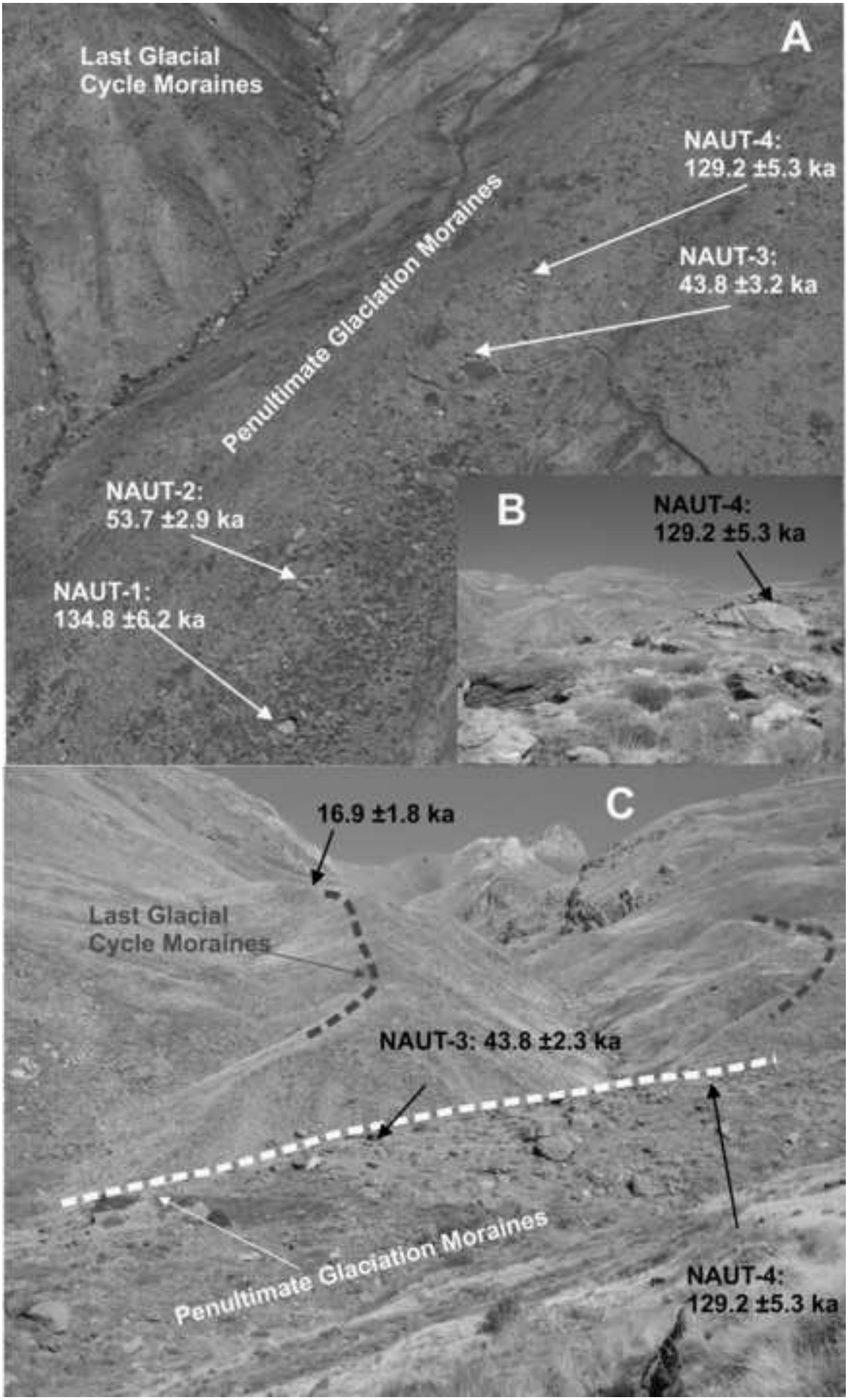

Figure (Greyscale)
Click here to download high resolution image

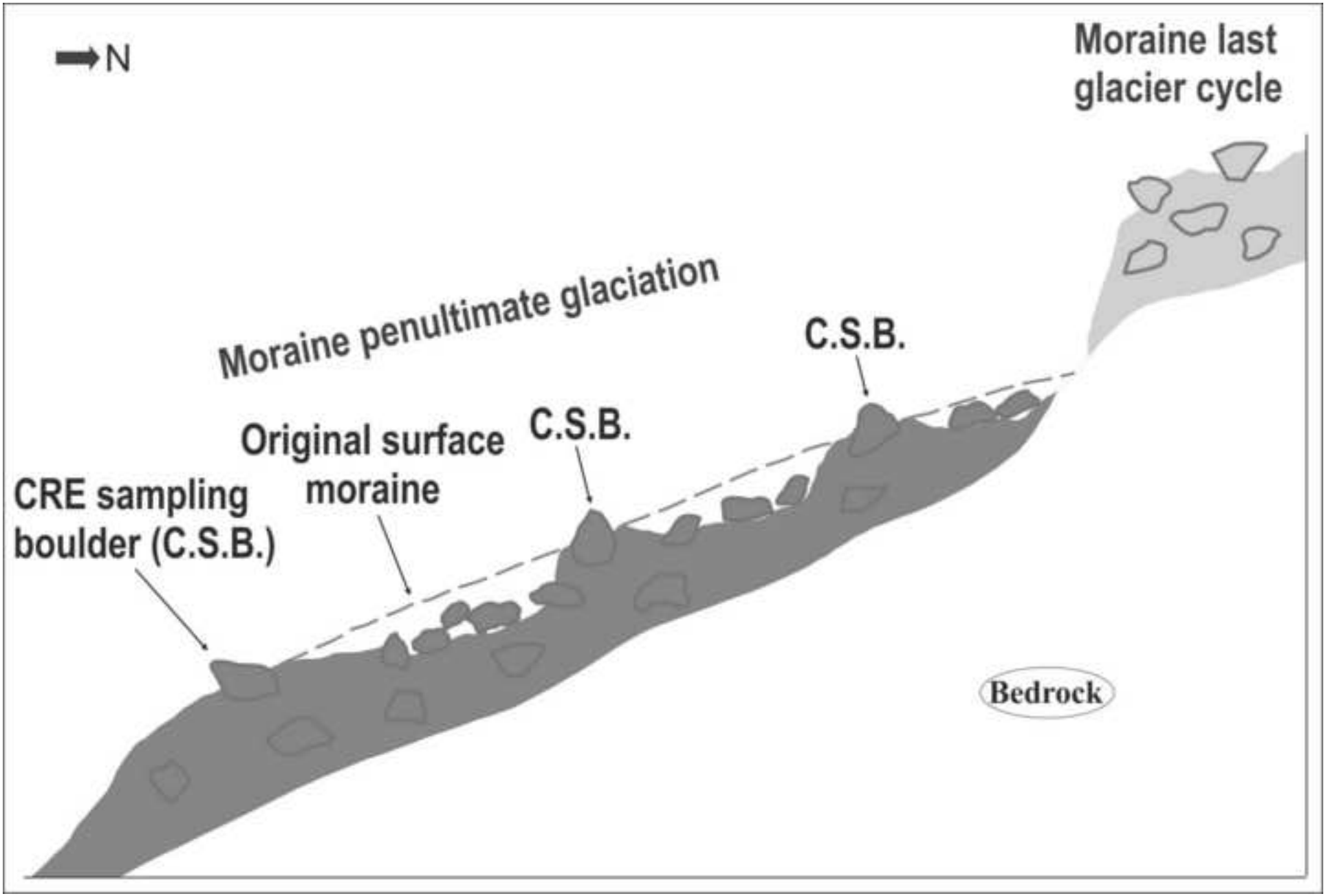

Figure (Greyscale)
Click here to download high resolution image

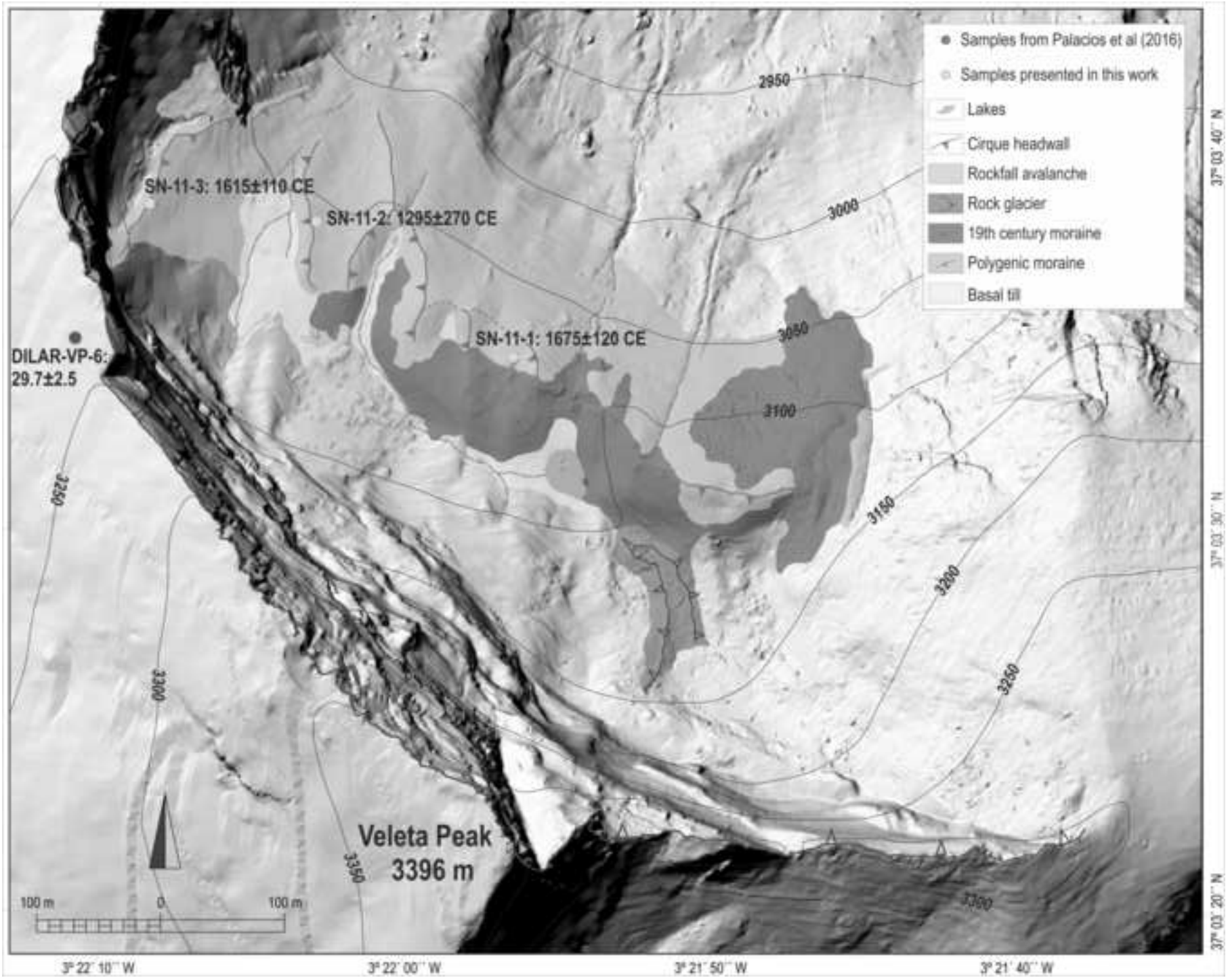

Figure (Greyscale)
Click here to download high resolution image

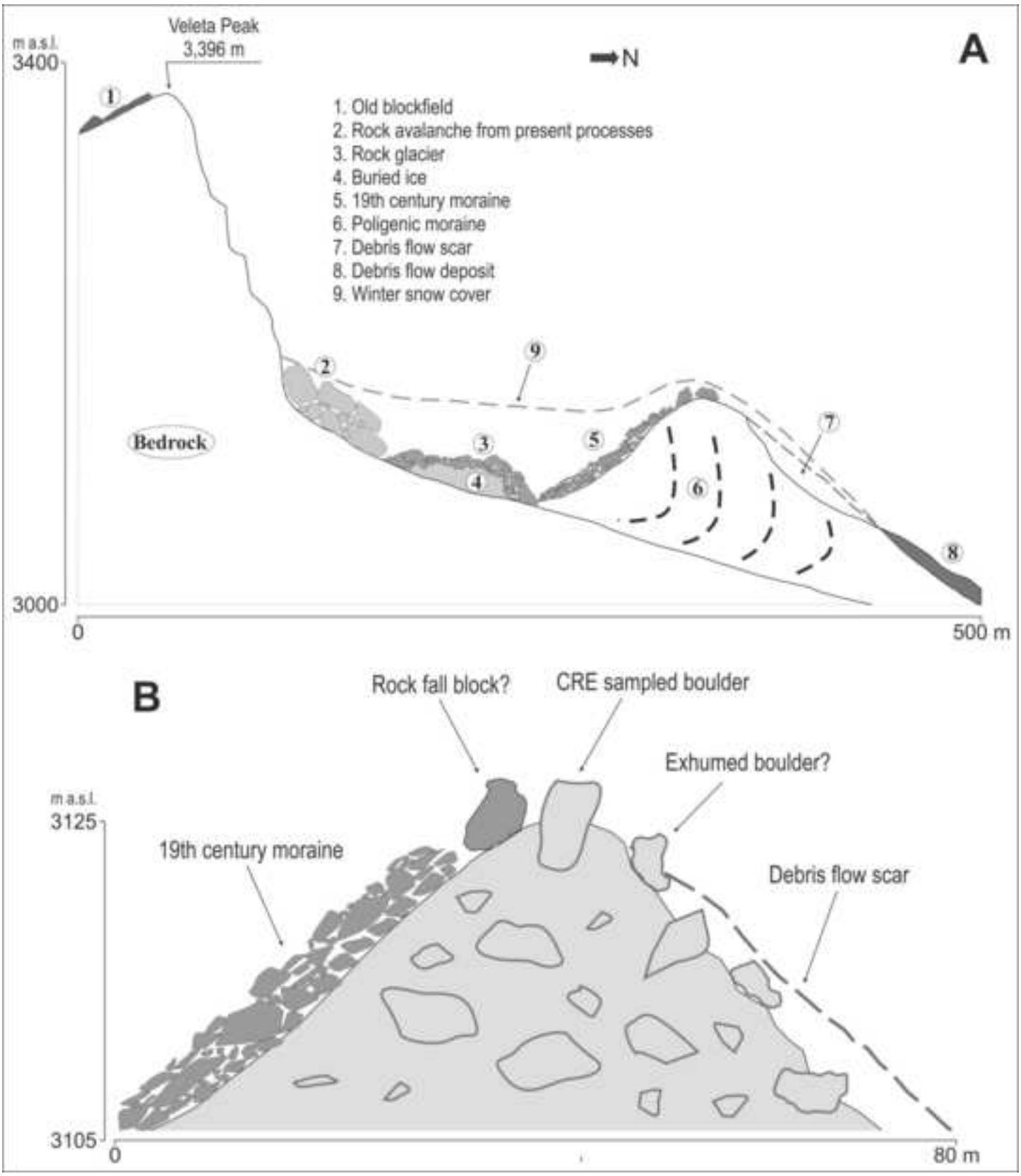

Figure (Greyscale)
Click here to download high resolution image

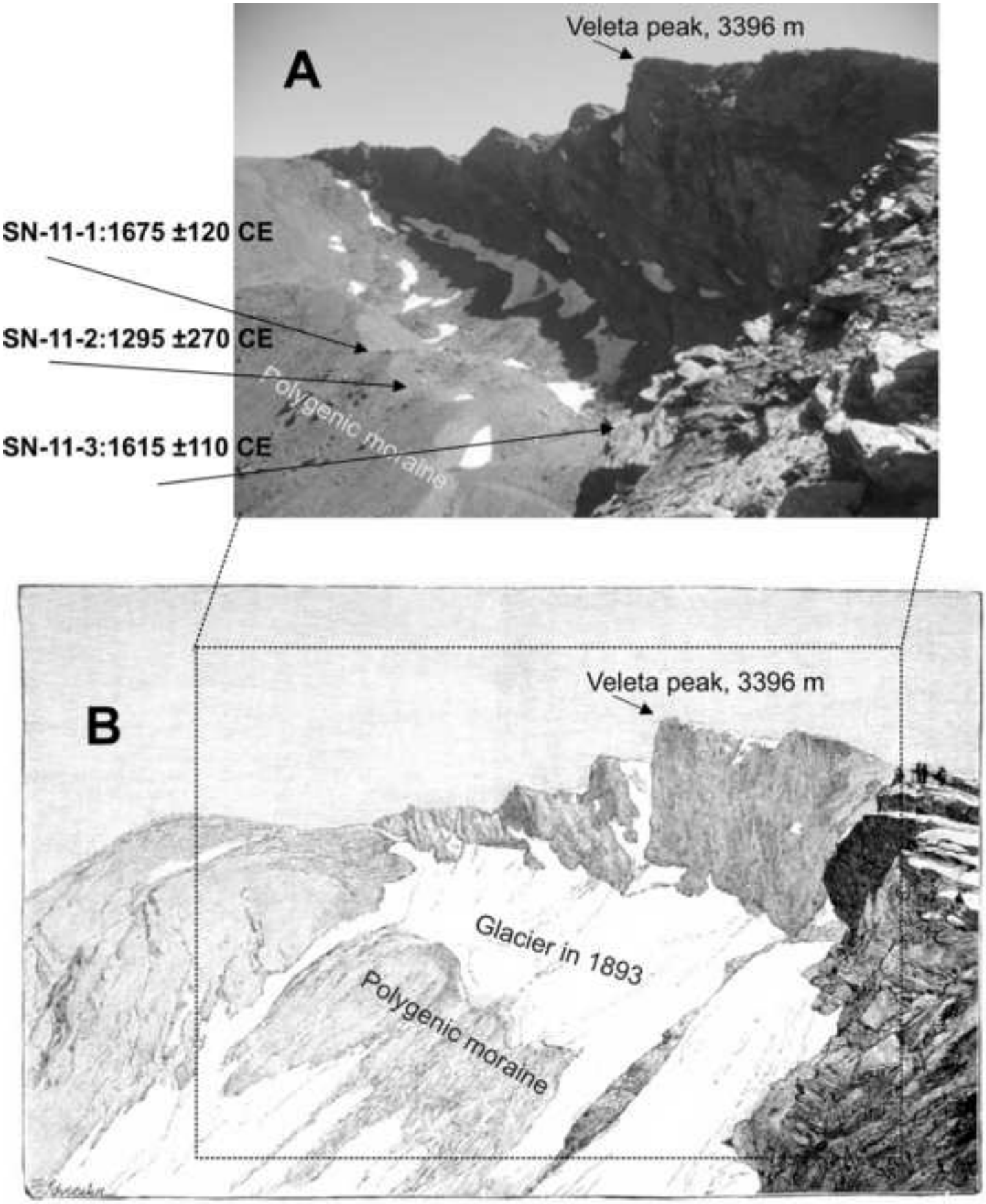

Figure (Greyscale)
Click here to download high resolution image

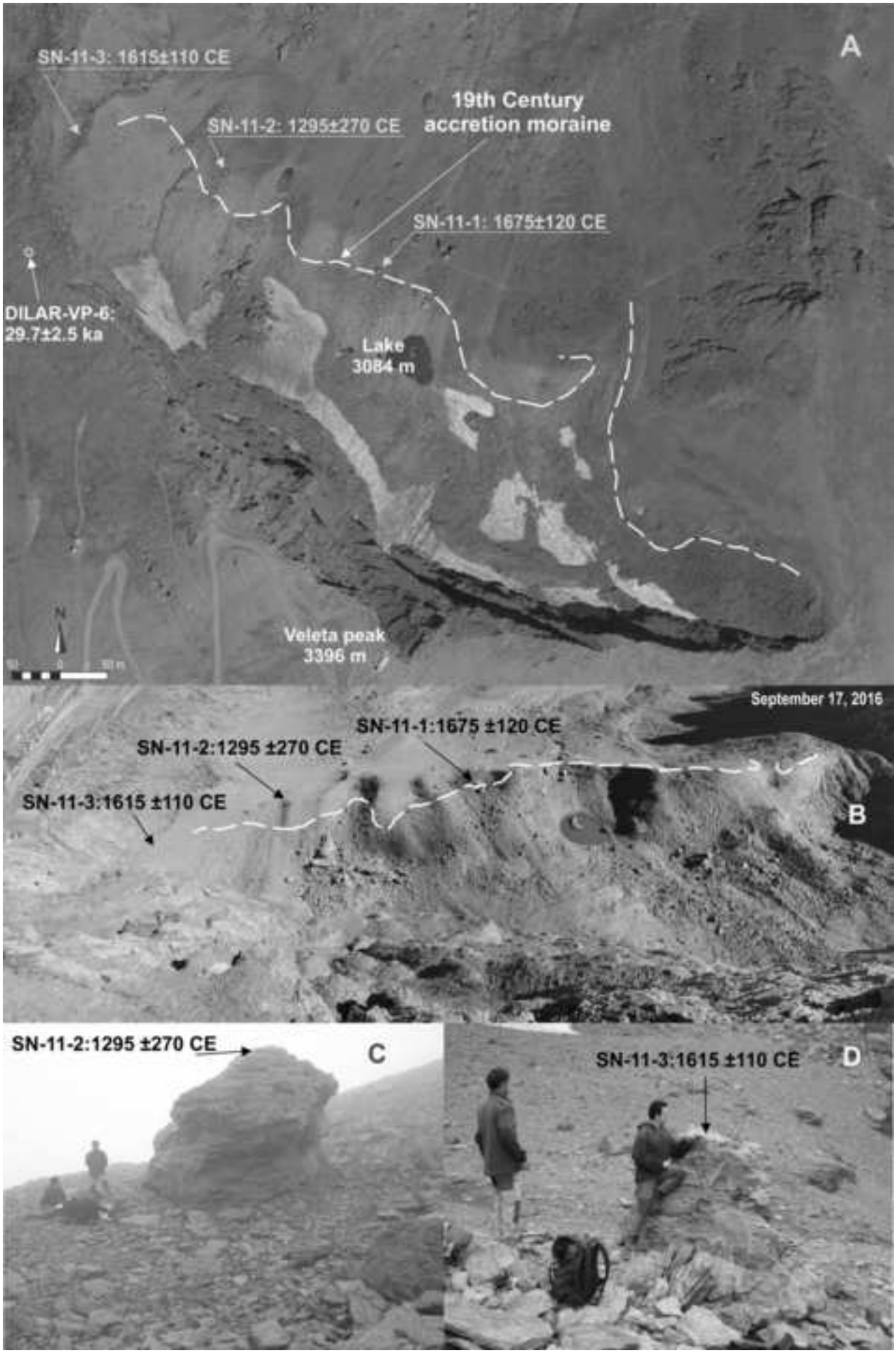

Figure (Greyscale)
Click here to download high resolution image

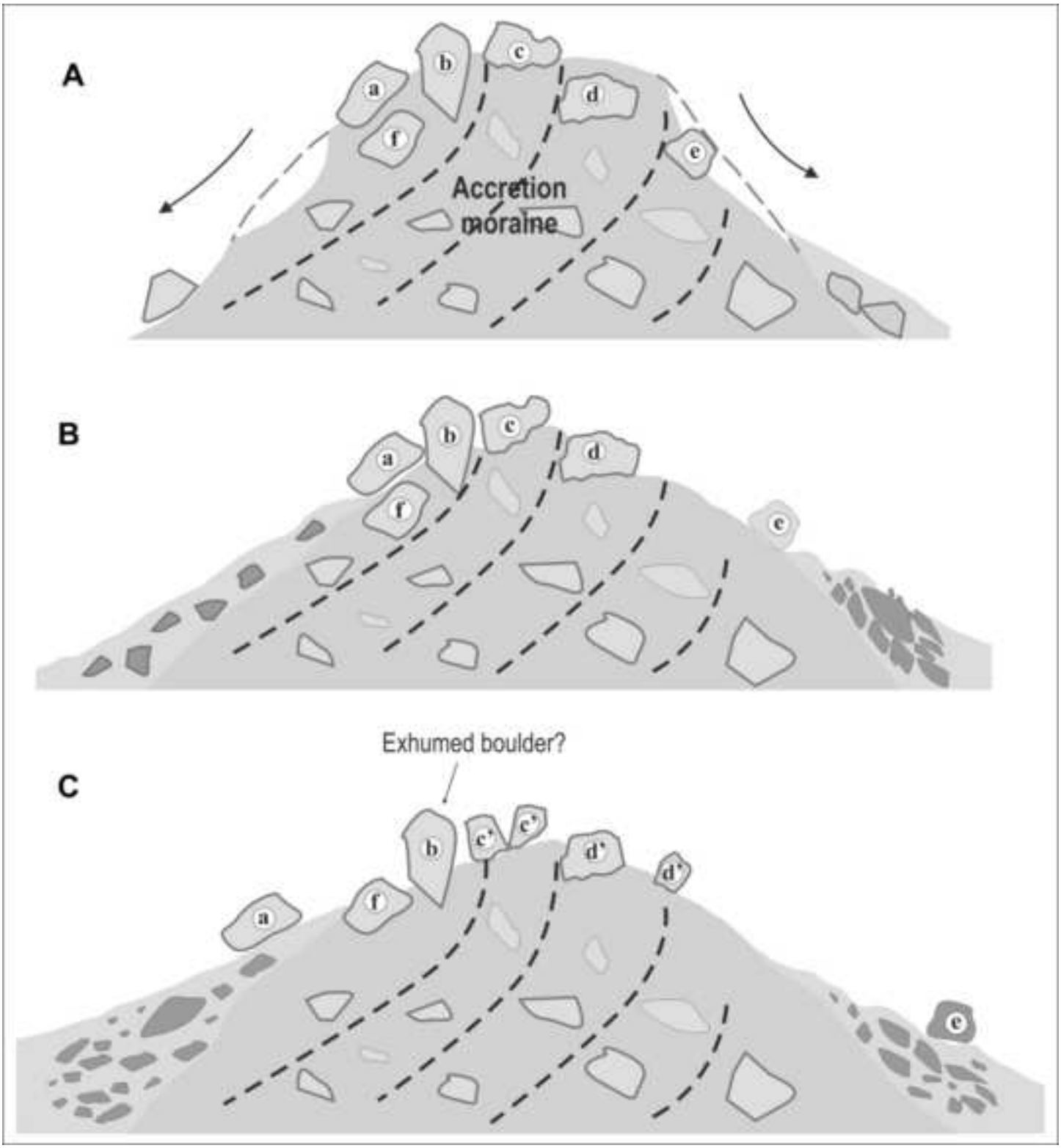

Click here to download Interactive Map file (.kml or .kmz): doc.kml